# Material Matters™

## Soft Electronics

## Sigma-Aldrich Presents:
## Flexible Futures

**POLYMER SEMICONDUCTORS**
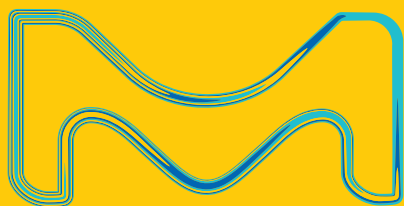for Intrinsically Stretchable
Organic Transistors

**ORGANIC OPTOELECTRONICS**
on Shape Memory Polymers

**ORGANIC PHOTOVOLTAIC APPLICATIONS**
for IoT, Architecture, and Wearables

**FLEXIBLE AND PRINTED ORGANIC
THERMOELECTRICS**: Opportunities
and Challenges

# Introduction

**Jia Choi, Ph.D.**
Product Manager,
Electronic Materials

Welcome to the third issue of *Material Matters*™ for 2017, focusing on high-performance stretchable and flexible electronic devices and functional electronic materials. There has been tremendous progress in the materials, designs, and manufacturing processes for stretchable and flexible systems, including transistors, biosensors, actuators, light emitting diodes, photodetector arrays, photovoltaics and integrated circuits. This issue of *Material Matters*™ provides an overview of the rapid advances in the design of stretchable and flexible electronic/optoelectronic devices and the use of functional organic electronic materials, in highly deformable devices.

In our first article, Dr. Zhenan Bao et al. (Stanford University, USA) highlight five different strategies for developing intrinsically stretchable polymer semiconductors for organic field-effect transistors (OFETs). These strategies help decrease polymer rigidity and crystallinity, resulting in softer and more ductile films that are essential for the development of implantable devices, a next generation bioelectronics.

Prof. Bernard Kippelen et al. (Georgia Institute of Technology, USA) in the second article provide a review of advances in the area of soft optoelectronics, with a focus on the development of organic optoelectronic devices on shape memory polymers (SMPs) for wearable electronic applications. The combination of the unique properties of SMP substrates with optoelectronics pave to the way for new applications, including conformable smart skin devices, minimally invasive biomedical devices, and flexible lighting/display technologies.

In the third article (EMD Performance Materials) provide a brief overview of organic photovoltaics (OPV) technologies as interesting energy-harvesting systems for use in the Internet of Things (IoT) and wearable electronics. Compared to existing power source alternatives, OPV offers added value in terms of performance, environmental-friendliness, custom-design, and form factor.

Dr. Jianguo Mei et al. (Purdue University, USA) in the final article discuss the opportunities and challenges of flexible and printed organic thermoelectronics. The authors focus on organic semiconductors such as n-type or p-type semiconducting polymers for use in flexible thermoelectronics.

Each article in this publication is accompanied by a list of relevant materials available from Aldrich Materials Science. For additional product information, visit us at **SigmaAldrich.com/matsci**. Please bother us with your new product suggestions, as well as thoughts and comments for *Material Matters*™ at **matsi@sial.com**.

## Welcome to the Future of *Material Matters*™

**Bryce P. Nelson, Ph.D.**
Materials Science
Initiative Lead

As part of the Merck KGaA, Darmstadt, Germany family, we're proud to grow as a company and better serve our customers. While you'll notice an evolution in the design of *Material Matters*™, the fundamental quality and trust that made Aldrich and Sigma-Aldrich a part of laboratories worldwide remains intact. We are confident that you will continue to find unique benefit in our scientists and collaborators for many years in the future. We have a new look and the same great articles. We continue to bring you the latest ideas and products to help drive your research. As always, previous issues of *Material Matters*™ are available online at **SigmaAldrich.com/mm**.

## About the Cover

Soft electronics uses organic and nano-scale materials to enable flexible and stretchable devices that can move while conforming to natural or curved shapes. Novel materials, advanced devices, and highly efficient processing platforms will be required to make these devices a reality. In this issue, our cover art expresses one of the very basic concepts in soft electronics, "flexible circuits".

# Table of Contents

## Articles

## Featured Products

# Your Material Matters

Ken Yoon, Ph.D
Head of Lab and Specialty Chemicals

*We welcome fresh product ideas. Do you have a material or compound you wish to see featured in our Materials Science line? If it is needed to accelerate your research, it matters. Send your suggestion to **matsci@sial.com** for consideration.*

Prof. Mark Hersam of Northwestern University recommended the addition of photonically annealable graphene ink for inkjet printing (**Cat. No. 900695**) to our catalog for use in printed and flexible electronics. Graphene is a remarkable material for printed electronics, offering a chemically stable, mechanically flexible, and electrically conductive alternative to conventional metal nanoparticle and conductive polymer inks.[1] The inkjet printing of graphene ink formulations using rapid intense pulsed light (IPL) annealing is well suited for rapid, roll-to-roll fabrication of graphene patterns on a variety of substrates.[2]

## References

(1)  Secor, E. B.; Prabhumirashi, P. L.; Puntambekar, K.; Geier, M. L.; Hersam, M. C. *J. Phys. Chem. Lett.* **2013**, *4*, 1347−1351
(2)  Secor, E. B.; Ahn, B. Y.; Gao, T. Z.; Lewis, J. A.; Hersam, M. C. *Adv. Mater.* **2015**, *27*, 6683–6688.

**Graphene dispersion**

Graphene ink; Conductive ink
inkjet printable, photonically annealable

| | |
|---|---|
| shear viscosity: | 7-14 mPa.s at 10 s$^{-1}$ (25 °C) |
| concentration: | 2.2-3.4 wt. % (graphene and ethyl cellulose in cyclohexanone/terpineol) |
| surface tension: | 28-36 dyn/cm |
| resistivity: | 0.003-0.008 Ω-cm, thermally annealed 300 °C for 30 minutes, film thickness >100 nm |
| density: | 0.9-1.1 g/mL, 25 °C |

| | |
|---|---|
| **900695-5ML** | 5 mL |

# Make it Bright.

**MilliporeSigma**

livilux® Organic Light Emitting Diode (OLED) materials are a unique portfolio of premium materials for OLEDs, from well-established materials to cutting-edge innovations.

## Key Features:
- Solution processibility
- Excellent reproducibility
- High efficiency
- Low operation voltage
- Long lifetime

The following livilux® OLED materials are now available at **SigmaAldrich.com**.

| Name | Description | Cat. No. |
|------|-------------|----------|
| PDY-132 | Super yellow light-emitting PPV copolymer | 900438 |
| PDO-123 | Orange light-emitting PPV copolymer | 900440 |
| SPG-01T | Green light-emitting spiro-copolymer | 900441 |
| SPR-001 | Red light-emitting spiro-copolymer, average $M_w$ 180,000 | 900444 |
| | Red light-emitting spiro-copolymer, average $M_w$ 470,000 | 900447 |
| | Red light-emitting spiro-copolymer, average $M_w$ 720,000 | 900446 |

To find out more about these products and our other OLED materials, visit **SigmaAldrich.com/oled**.

# Polymer Semiconductors for Intrinsically Stretchable Organic Transistors

Ging-Ji Nathan Wang, Zhenan Bao*

Department of Chemical Engineering, Stanford University, Stanford, CA 94305-5025, USA
*E-mail: zbao@stanford.edu

## Introduction

Stretchable Electronics is an emerging field in organic electronics that is experiencing rapid growth due to its application in wearable and implantable devices.[1,2] While stretchable interconnects and induced "buckling" have been used to fabricate stretchable light emitting diodes (LEDs),[3] solar cells,[4] and transistors[5] using rigid components, the development of intrinsically stretchable semiconductors is essential for the realization of low cost, high density devices. Semiconducting polymers are attractive candidates for the fabrication of intrinsically stretchable electronics for several reasons. First, they have a relatively low tensile modulus (~1 GPa or lower) compared to that of silicon and inorganic semiconductors (~100 GPa), which provides a softer interface suitable for bioelectronics. Second, advancements in organic chemistry make these materials highly tunable, and thus bio-compatible and bio-degradable if desired.[6] Since they are polymer plastics, they possess great potential for the development of tough, elastic and self-healing properties via polymer chain entanglement, crosslinking, and non-covalent interactions (not to mention that most biological tissues are polymeric in nature). Finally, these materials are solution processable, allowing them to be printed and patterned over large areas.

However, the major challenge in developing semiconducting polymers is simultaneously maintaining both stretchability and good semiconducting properties. Since extended π-conjugation on the polymer backbone is vital for good electronic properties, semiconducting polymers are often rigid and semicrystalline. This is especially apparent in field-effect transistors, which typically require a highly crystalline semiconductor to obtain high charge-carrier mobility. A number of approaches have been reported to improve both characteristics, including side-chain modification,[7] backbone fragmentation,[8] embedding semiconducting nanofibers in styrene-ethylene/butylene-styrene (SEBS, **Cat. Nos. 200557 and 200565**),[9] and blending high-mobility polymers with ductile semiconductors.[10] While these approaches have successfully improved the mechanical compliance of conjugated polymers, maintaining high transport mobility remains a challenge.

Herein we present a few examples of our group's work on intrinsically stretchable active layers for organic field-effect transistors (OFET), showcasing our contributions in the past few years toward the development of stretchable electronics. These approaches can be divided into two categories: polymer structural modification and post-polymerization modifications. The first concentrates on the design of the conjugated polymer including the choice of polymer backbone and side-chain, as well as the introduction of non-covalent interactions. The second focuses on strategies that can be applied to polymer semiconductors in general such as crosslinking and blending with insulating but stretchable polymeric materials.

## Polymer Structural Modifications

The difference in mechanical properties of semiconducting polymers was first highlighted by DeLongchamp et al. when comparing P3HT (**Cat. Nos. 445703, 900549, 900563,** and **900550**) and pBTTT (**Cat. No. 753971**).[11] Where a direct relationship between field-effect mobility ($\mu^{FET}$) and modulus was shown. For example, moderately crystalline P3HT exhibited low $\mu^{FET}$ and highly crystalline pBTTT exhibited high $\mu^{FET}$ and modulus due to its interdigitated side-chains. However, a better understanding of charge transport in conjugated polymers in recent years has prompted the development of low crystallinity and high $\mu^{FET}$ polymers.[12] For example, Salleo et al. shownned that long-range charge transport can be achieved using poorly ordered polymers with high molecular weight and good intermolecular aggregation, contrary to traditional views.[13]

### Highly Aggregating Donor-Acceptor Polymers

Inspired by the previously mentioned understanding, we have focused on Donor-Acceptor (D-A) type polymers, which are known to aggregate and possess excellent charge-carrier mobility. We demonstrated using an internally developed soft contact lamination method that PiI-2T has comparable mechanical properties as P3HT but a higher $\mu^{FET}$ of $1.52 \times 10^{-2}$ cm$^2$V$^{-1}$s$^{-1}$ at 100% strain shown in **Figure 1B**.[14] Unfortunately, the PDPP-FT4 investigated showed poor stretchability despite superior charge transport.

**A)**



**B)**
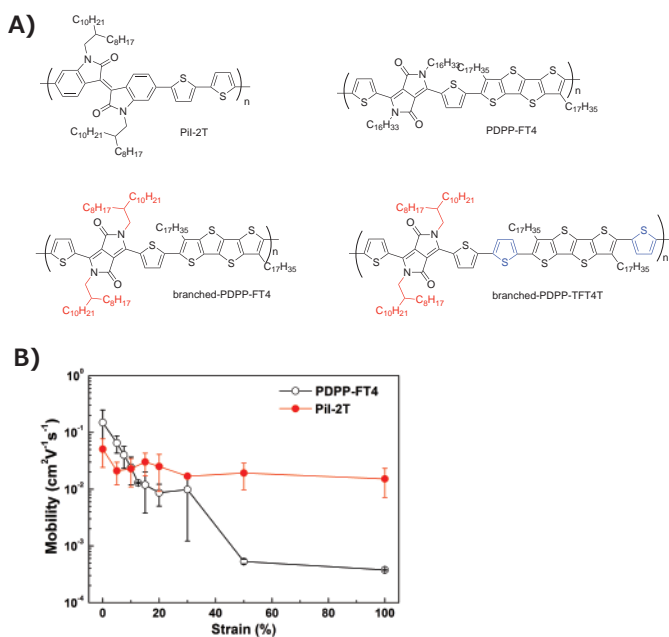


**Figure 1.** A) Chemical Structures of PiI-2T, PDPP-FT4, branched-PDPP-FT4 and branched-PDPP-TFT4T. B) $\mu^{FET}$ of PDPP-FT4 and PiI-2T measured by soft-contact lamination method for various amounts of strain applied. Adapted with permission. Copyright 2014 American Chemistry Society.[14]

## Back-bone and Side-chain Modification

To further account for the poor mechanical properties of PDPP-FT4 and establish general design rules for stretchable D-A polymers, we considered two additional DPP-type polymers: branched-PDPP-FT4 with branched side-chains and branched-PDPP-TFT4T with branched side-chains and additional thiophene spacers between the fused tetrathienoacene as highlighted in **Figure 1A**.[15] By measuring the tensile modulus and fabricating OFET from stretched polymer films we observed a decrease in modulus and an increase in ductility when incorporating branched side-chains. Furthermore, upon the addition of thiophene spacers, the polymer film did not show crack propagation until 40% strain and maintained a hole mobility of 0.1 cm$^2$V$^{-1}$s$^{-1}$ up to 100% strain. This was attributed to the decrease in crystallinity and the entangled nonfibrillar texture observed by grazing-incidence X-ray diffraction (GIXD) and atomic force microscopy (AFM). With careful backbone and side-chain engineering we could manipulate a polymer's molecular packing and backbone rigidity while maintaining good charge transport.

## Stress Dissipation and Healing Mechanism through Hydrogen Bonding

Introducing an energy dissipating mechanism is another effective strategy to impart stretchability.[16] Following our previous work that displayed a highly stretchable and self-healing elastomer,[17] we incorporated a 2,6-pyridine dicarboxamide (PDCA) unit with moderate hydrogen bonding (H-bonding) strength to a DPP polymer to give PDPP-TVT-10PDCA shown in **Figure 2A**.[18]

Compared to the control polymer PDPP-TVT, the PDCA polymer displayed a decrease in tensile modulus and an increase in fracture strain at 120% strain. Transistors prepared from strained polymer films gave a stable $\mu^{FET}$ above 1.0 cm$^2$V$^{-1}$s$^{-1}$ up to 100% strain. **Figure 2B** shows the high durability of the polymer active layer which only showed a 26% decrease in $\mu^{FET}$ after 100 cycles of rigorous stretching at 100% strain. This improvement in toughness was attributed to the weak H-bonding from the PDCA unit which acts as a sacrificial bond and breaks upon strain, hence releasing stress experienced by the polymer chains.

Additionally, the dynamic nature of the H-bonding allowed the PDPP-TVT-10PDCA film to heal upon solvent and thermal annealing. **Figure 2E** shows the AFM images of the damaged film after stretching and the recovered film after solvent and thermal annealing. Clear nanocracks were observed initially, but after the healing treatment, cracks were no longer apparent and the $\mu^{FET}$ recovered back to above 1.0 cm$^2$V$^{-1}$s$^{-1}$. This is the first demonstration of a semiconducting polymer with healing capability.

## Post-polymerization Modifications

Aside from modifying monomer structures, there are numerous post-polymerization modifications that can alter a material's intrinsic mechanical properties, such as adding plasticizers, physical blending, crosslinking, hydrogenation, etc. While these techniques have been used for decades, very few have been tested with conjugated polymers. The advantage of post-polymerization modifications is their applicability to a variety of polymer semiconductors. This gives us an opportunity to convert brittle materials with good $\mu^{FET}$ to stretchable materials.

## Crosslinking with Oligo-siloxanes

Decreasing backbone rigidity and increasing amorphous regions yields softer semiconductors with enhanced ductility. However, to improve the elasticity and fatigue resistance of a material, some form of crosslinking is required to prevent irreversible deformation upon strain. To test this, we crosslinked a DPP random co-polymer containing 20% crosslinkable side-chains (20DPPTTEC) with a PDMS oligomer to give 20DPPTTECx.[19] The crosslinked film showed an increase in yield strain from 8% to 14% strain as determined by the buckling onset strain. More importantly, no cracks were observed even after 500 cycles of 100% strain. **Figure 3D** shows the height profile of the strained polymer film; 40 nm deep cracks and 60 nm tall wrinkles were formed in the pristine film, whereas 20 nm tall wrinkles were found in the crosslinked film, highlighting the improved elasticity. To assess the fatigue resistance of the polymer films, they were subjected to cyclic loading of 20% strain. The pristine polymer started showing decay in $\mu^{FET}$ after 10 cycles of 20% strain whereas the crosslinked films maintained a $\mu^{FET}$ of 0.4 cm$^2$V$^{-1}$s$^{-1}$ up to 500 cycles. Interestingly, the siloxane crosslinkers also showed a plasticizing effect, which accounted for a decrease in tensile modulus and crystallinity as observed by GIXD.
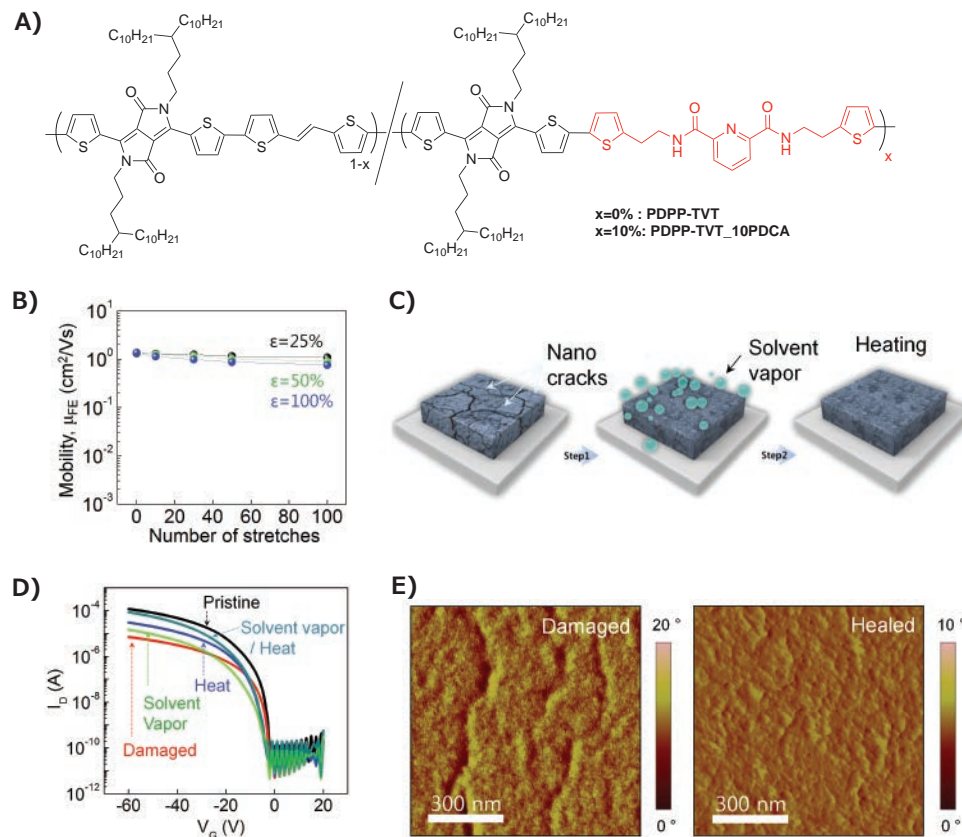
**Figure 2.** A) Chemical structures of PDPP-TVT and PDPP-TVT-10PDCA. B) $\mu^{FET}$ of PDPP-TVT-10PDCA versus number of stretching cycles performed perpendicular to strain direction in bottom-gate-top-contact device configuration. C) Schematic representation of the treatments used for healing the conjugated polymer films. D) Transfer curves of damaged and healed PDPP-TVT-10PDCA OFET. E) AFM phase image for damaged and healed film of PDPP-TVT-10PDCA. Reproduced with permission. Copyright 2016, Nature Publishing Group.[18]
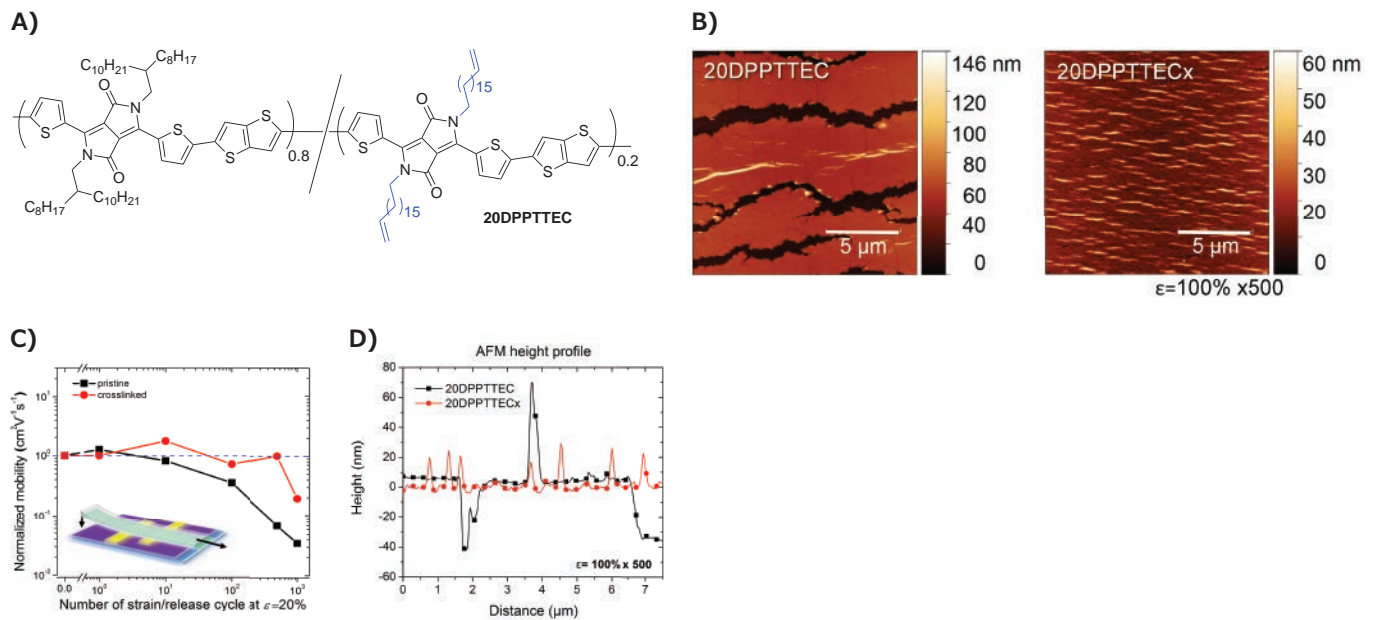


**Figure 3.** A) Chemical structure of 20DPPTTEC. B) AFM height image of 20DPPTTEC and 20DPPTTECx relaxed from 500 cycles of 100% strain. C) Normalized $\mu^{FET}$ of 20DPPTTEC and 20DPPTTECx versus number of stretching cycles at 20% strain performed perpendicular to strain direction. D) AFM height profile of 20DPPTTEC and 20DPPTTECx after 500 cycles of 100% strain. The crosslinked polymer forms 20 nm tall wrinkles upon cyclic loading, whereas the pristine polymer forms microcracks and 60 nm tall wrinkles. Reproduced with permission. Copyright 2016 Wiley-VCH.[19]

## Nanoconfinement through Blending with SEBS Polymer

While nanoconfinement is a known strategy to alter a polymer's ductility, chain dynamics, and modulus, it had never been previously studied using conjugated polymers. By blending conjugated polymer DPPT-TT (**Cat. No. 791989**) with 70 weight % of SEBS, we obtained polymer films that showed vast improvement in mechanical properties while maintaining excellent electrical properties.[20] The comparable surface energies of the semiconductor and elastomer leads to a nanoscale phase-separation upon blending as shown in **Figure 4B**. The confinement effect from the SEBS matrix suppresses crystallization in the film and decreases the glass transition temperature of the polymer, which leads to a decrease in modulus and increase in fracture and yield strain. The blended film could be stretched to 100% strain with no cracks and no apparent decrease in $\mu^{FET}$. To date, almost all stretchable polymer active layers show compromise in $\mu^{FET}$ when compared to their parent polymer. However, our SEBS-polymer blend showed no degradation in electrical properties when compared with the pristine DPPT-TT semiconductor. This is due to the strong aggregation that is maintained in the polymer blend despite a decrease in crystallinity. Furthermore, the SEBS could impart elastic properties to the polymer film, showing stable $\mu^{FET}$ up to 1,000 cycles of 25% strain. **Figure 4C** shows the drain current from the fully stretchable transistor under stretching, twisting, and poking by sharp object. The stable drain current demonstrates the robustness of the device prepared from the polymer blend. Finally, the general applicability of this method was tested with various conjugated polymers. Of the additional four polymer semiconductors tested, three could achieve $\mu^{FET}$ above 1.0 $cm^2V^{-1}s^{-1}$ under 100% strain and none of the polymers displayed cracks under optical microscopy. **Figure 4D** shows the improvement in mobility of each polymer under nanoconfinement at 100% strain. Even the brittle PDPP-FT4 discussed earlier showed uniform films under strain and four orders of magnitude increase in $\mu^{FET}$.

## Conclusions

In this article, we have summarized five different strategies for developing intrinsically stretchable polymer semiconductors for OFET. This includes utilizing the high $\mu^{FET}$ and aggregating properties of D-A polymers, side-chain and backbone engineering, the addition of H-bonding moieties, covalent crosslinking, and the introduction of nanoconfinement via SEBS blends. These approaches have successfully allowed us to decrease polymer rigidity and crystallinity, resulting in softer and more ductile films. Film toughness and elasticity were also greatly improved, giving greater fracture strains and fatigue resistance. H-bonding units further allowed films to heal from nanocracks upon solvent and thermal annealing. Soft, healable, robust, and intrinsically stretchable transistors are essential steps towards the development of implantable devices as well as next generation bioelectronics.
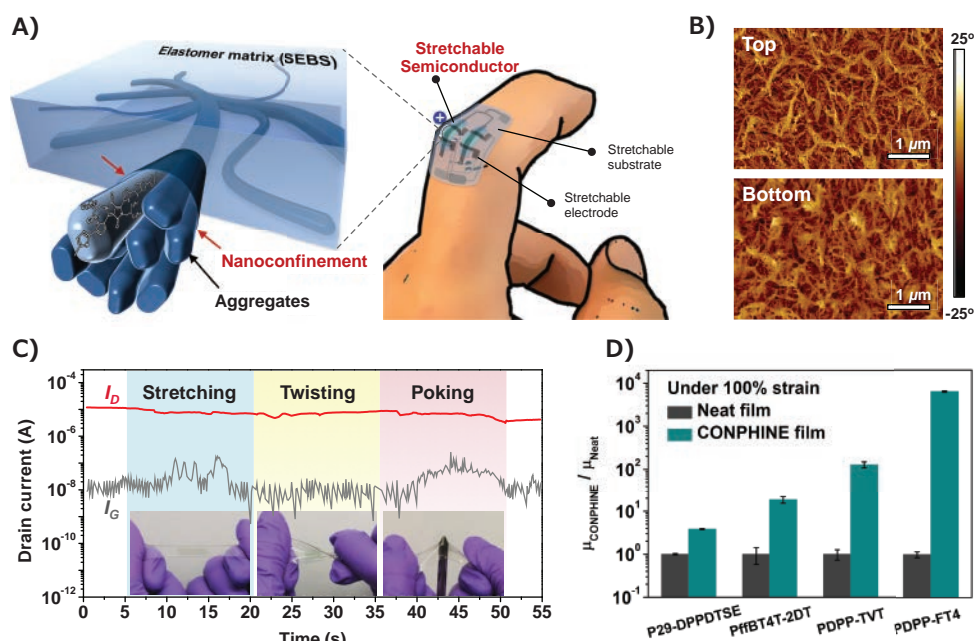


**Figure 4.** A) A 3D schematic of the desired morphology composed of embedded nanoscale networks of polymer semiconductor, which can be used to construct a highly stretchable and wearable OFET. B) AFM phase images of the top and bottom interface of the nanoconfined film with 70 wt % SEBS and 30 wt % DPPT-TT. C) Drain current (ID) and gate current (IG) of a fully stretchable transistor under sequential stretching, twisting, and poking with a sharp object. D) Normalized µFET of neat films (gray) and the corresponding blended film of these conjugated polymer, under 100% strain. Reproduced with permission. Copyright 2017 AAAS.[19]
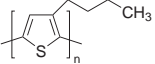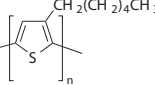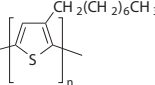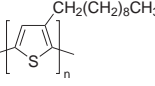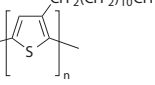
## References

(1) Lipomi, D. J.; Bao, Z. *MRS Bull*. **2017**, *42*(2), 93–97.
(2) Someya, T.; Bao, Z.; Malliaras, G. G. *Nature* **2016**, *540*(7633), 379–385.
(3) White, M. S.; Kaltenbrunner, M.; Głowacki, E. D.; Gutnichenko, K.; Kettlgruber, G.; Graz, I.; Aazou, S.; Ulbricht, C.; Egbe, D. A. M.; Miron, M. C.; Major, Z.; Scharber, M. C.; Sekitani, T.; Someya, T.; Bauer, S.; Sariciftci, N. S. *Nat. Photonics* **2013**, *7*(10), 811–816.
(4) Lipomi, D. J.; Tee, B. C.-K.; Vosgueritchian, M.; Bao, Z. *Adv. Mater*. **2011**, *23*(15), 1771–1775.
(5) Kim, D.-H.; Ahn, J.-H.; Choi, W. M.; Kim, H.-S.; Kim, T.-H.; Song, J.; Huang, Y. Y.; Liu, Z.; Lu, C.; Rogers, J. A. *Science* **2008**, *320*(5875), 507–511.
(6) Irimia-Vladu, M.; Troshin, P. A.; Reisinger, M.; Shmygleva, L.; Kanbur, Y.; Schwabegger, G.; Bodea, M.; Schwödiauer, R.; Mumyatov, A.; Fergus, J. W.; Razumov, V. F.; Sitter, H.; Sariciftci, N. S.; Bauer, S. *Adv. Funct. Mater*. **2010**, *20*(23), 4069–4076.
(7) Savagatrup, S.; Printz, A. D.; Rodriquez, D.; Lipomi, D. J. *Macromolecules* **2014**, *47*(6), 1981–1992.
(8) Printz, A. D.; Savagatrup, S.; Burke, D. J.; Purdy, T. N.; Lipomi, D. J. *RSC Adv*. **2014**, *4*(26), 13635.
(9) Shin, M.; Oh, J. Y.; Byun, K.-E.; Lee, Y.-J.; Kim, B.; Baik, H.-K.; Park, J.-J.; Jeong, U. *Adv. Mater*. **2015**, *27*(7), 1255–1261.
(10) Sun, T.; Scott, J. I.; Wang, M.; Kline, R. J.; Bazan, G. C.; Connor, B. T. O. *Adv. Electron. Mater.* **2017**, *3*, 1600388.
(11) O'Connor, B.; Chan, E. P.; Chan, C.; Conrad, B. R.; Richter, L. J.; Kline, R. J.; Heeney, M.; McCulloch, I.; Soles, C. L.; DeLongchamp, D. M. *ACS Nano* **2010**, *4*(12), 7538–7544.
(12) Zhang, X.; Bronstein, H.; Kronemeijer, A. J.; Smith, J.; Kim, Y.; Kline, R. J.; Richter, L. J.; Anthopoulos, T. D.; Sirringhaus, H.; Song, K.; Heeney, M.; Zhang, W.; McCulloch, I.; DeLongchamp, D. M. *Nat. Commun.* **2013**, *4*, 1–9.
(13) Noriega, R.; Rivnay, J.; Vandewal, K.; Koch, F. P. V.; Stingelin, N.; Smith, P.; Toney, M. F.; Salleo, A. *Nat. Mater.* **2013**, *12*(11), 1038–1044.
(14) Wu, H.-C.; Benight, S. J.; Chortos, A.; Lee, W.-Y.; Mei, J.; To, J. W. F.; Lu, C.; He, M.; Tok, J. B.-H.; Chen, W.-C.; Bao, Z. *Chem. Mater.* **2014**, *26*(15), 4544–4551.
(15) Lu, C.; Lee, W.; Gu, X.; Xu, J.; Chou, H.; Yan, H.; Chiu, Y.; He, M.; Matthews, J. R.; Niu, W.; Tok, J. B.-H.; Toney, M. F.; Chen, W.; Bao, Z. *Adv. Electron. Mater.* **2016**, 201600311, 1600311.
(16) Sun, J.-Y.; Zhao, X.; Illeperuma, W. R. K.; Chaudhuri, O.; Oh, K. H.; Mooney, D. J.; Vlassak, J. J.; Suo, Z. *Nature* **2012**, *489*(7414), 133–136.
(17) Li, C.-H.; Wang, C.; Keplinger, C.; Zuo, J.-L.; Jin, L.; Sun, Y.; Zheng, P.; Cao, Y.; Lissel, F.; Linder, C.; You, X.-Z.; Bao, Z. *Nat. Chem.* **2016**, *8*, 618–624.
(18) Young Oh, J.; Rondeau-Gagné, S.; Chiu, Y.; Chortos, A.; Lissel, F.; Wang, G.-J. N.; Schroeder, B. C.; Kurosawa, T.; Lopez, J.; Katsumata, T.; Xu, J.; Zhu, C.; Gu, X.; Bae, W.; Kim, Y.; Jin, L.; Won Chung, J.; B-H Tok, J.; Bao, Z. *Nature* **2016**, *539*(7629), 411–415.
(19) Wang, G.-J. N.; Shaw, L.; Xu, J.; Kurosawa, T.; Schroeder, B. C.; Oh, J. Y.; Benight, S. J.; Bao, Z. *Adv. Funct. Mater.* **2016**, *26* (40), 7254–7262.
(20) Xu, J.; Wang, S.; Wang, G.-J. N.; Zhu, C.; Luo, S.; Jin, L.; Gu, X.; Chen, S.; Feig, V. R.; F To, J. W.; Rondeau-Gagné, S.; Park, J.; Schroeder, B. C.; Lu, C.; Young Oh, J.; Wang, Y.; Kim, Y.; Yan, H.; Sinclair, R.; Zhou, D.; Xue, G.; Murmann, B.; Linder, C.; Cai, W.; B-H Tok, J.; Won Chung, J.; Bao, Z. *Science* **2017**, *355*(6320), 59–64.
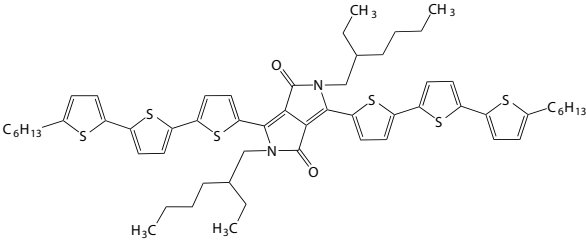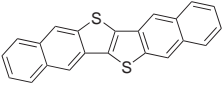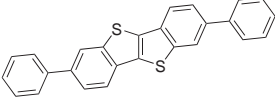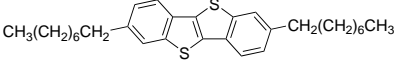
## Poly(3-alkylthiophene-2,5-diyl)
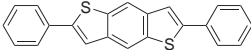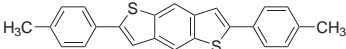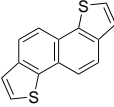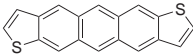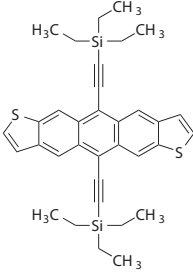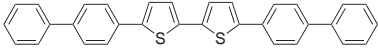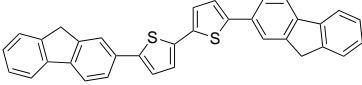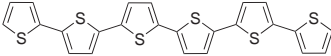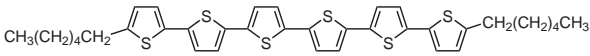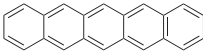
For a complete list of available materials, visit **SigmaAldrich.com/polythio**.
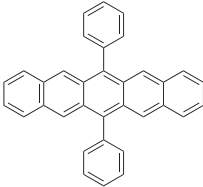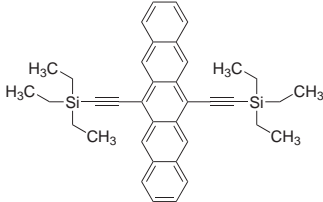
| Name | Structure | Regioregularity | Molecular Weight | Cat. No. |
|---|---|---|---|---|
| Poly(3-butylthiophene-2,5-diyl) | | regioregular | $M_w$ 54,000 (typical) | **495336-1G** |
| | | regiorandom | - | **511420-1G** |
| Poly(3-hexylthiophene-2,5-diyl) | | regioregular | average $M_w$ 50,000-100,000 | **445703-1G** |
| | | | average $M_w$ 20,000-45,000 | **900563-1G** **900563-5G** |
| | | | average $M_w$ 50,000-75,000 | **900550-1G** **900550-5G** |
| | | | average $M_w$ 85,000-100,000 | **900549-1G** |
| | | regiorandom | - | **510823-1G** |
| Poly(3-octylthiophene-2,5-diyl) | | regioregular | average $M_n$ ~25,000 | **682799-250MG** |
| | | | average $M_n$ ~34,000 | **445711-1G** |
| | | regiorandom | average $M_n$ 22,000 average $M_w$ 36,600 | **510831-1G** |
| Poly(3-decylthiophene-2,5-diyl) | | regioregular | average $M_n$ ~30,000 average $M_w$ ~42,000 | **495344-1G** |
| Poly(3-dodecylthiophene-2,5-diyl) | | regioregular | average $M_w$ ~60,000 | **450650-1G** |
| | | regiorandom | average $M_n$ 30,000 average $M_w$ 70,000 | **510866-1G** |

## P-type Small Molecules

For a complete list of available materials, visit **SigmaAldrich.com/psmall**.
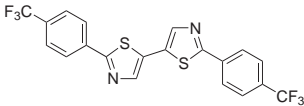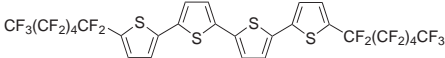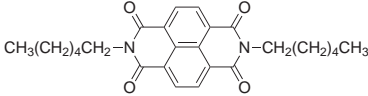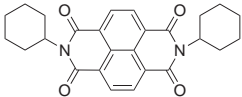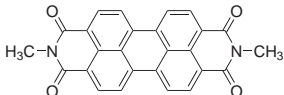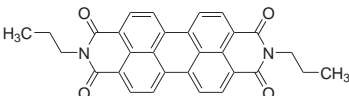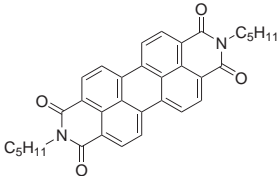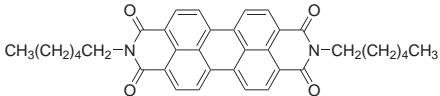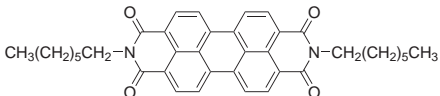
| Name | Structure | Purity | Mobility | Cat. No. |
|---|---|---|---|---|
| SMDPPEH | | 97%, HPLC | ~$10^{-4}$ cm²/V·s | **753912-250MG** |

| Name | Structure | Purity | Mobility | Cat. No. |
|------|-----------|--------|----------|----------|
| Dinaphtho[2,3-b:2′,3′-f]thieno[3,2-b]thiophene | | 99%, sublimed grade | 2 cm²/V·s | **767638-100MG**<br>**767638-500MG** |
| 2,7-Diphenyl[1]benzothieno[3,2-b][1]benzothiophene | | 99%, sublimed grade | 2 cm²/V·s | **767603-100MG**<br>**767603-500MG** |
| C8-BTBT | $CH_3(CH_2)_6CH_2$ — ... — $CH_2(CH_2)_6CH_3$ | ≥99%, HPLC | 5.5 cm²/V·s | **747092-100MG**<br>**747092-250MG** |
| 2,6-Diphenylbenzo[1,2-b:4,5-b′]dithiophene | | 97%, sublimed grade | $4.6\times10^{-3}$ cm²/V·s | **767611-100MG**<br>**767611-500MG** |
| 2,6-Ditolylbenzo[1,2-b:4,5-b′]dithiophene | $H_3C$ — ... — $CH_3$ | 95%, sublimed grade | $10^{-2}$ cm²/V·s | **767646-100MG**<br>**767646-500MG** |
| Naphtho[1,2-b:5,6-b′]dithiophene | | 97% | >0.5 cm²/V·s | **768677-500MG** |
| ADT | | 97% | 0.3 cm²/V·s | **754080-250MG** |
| TES-ADT | | >99%, HPLC | 1 cm²/V·s | **754102-100MG** |
| 5,5′-Di(4-biphenylyl)-2,2′-bithiophene | | 97% | 0.04 cm²/V·s | **695947-1G** |
| FTTF | | sublimed grade | 0.3 cm²/V·s | **754056-250MG** |
| DH-FTTF | $C_6H_{13}$ — ... — $C_6H_{13}$ | 95% | 0.05-0.12 cm²/V·s | **754064-250MG** |
| α-Sexithiophene | | - | 0.075 cm²/V·s | **594687-1G** |
| 5,5‴″-Dihexyl-2,2′:5′,2″:5″,2‴:-5‴,2″″:5″″,2″″′-sexithiophene | $CH_3(CH_2)_4CH_2$ — ... — $CH_2(CH_2)_4CH_3$ | - | 0.13 cm²/V·s | **633216-500MG** |
| Pentacene | | ≥99.995% trace metals basis, triple-sublimed grade | 0.4-3 cm²/V·s | **698423-500MG** |
| | | ≥99.9% trace metals basis, sublimed grade | 0.4-3 cm²/V·s | **684848-1G** |
| | | 99% | 0.4-3 cm²/V·s | **P1802-100MG**<br>**P1802-1G**<br>**P1802-5G** |

| Name | Structure | Purity | Mobility | Cat. No. |
|---|---|---|---|---|
| 6,13-Diphenylpentacene | | 98% | $8\times10^{-5}$ cm²/V·s | **760641-1G** |
| 6,13-Bis((triethylsilyl)ethynyl) pentacene | | ≥99%, HPLC | $10^{-5}$ cm²/V·s | **739278-100MG**<br>**739278-500MG** |

## N-type Small Molecules
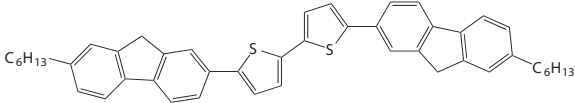
For a complete list of available materials, visit **SigmaAldrich.com/nsmall**.

| Name | Structure | Purity | Mobility | Cat. No. |
|---|---|---|---|---|
| 2,2′-Bis[4-(trifluoromethyl)phenyl]-5,5′-bithiazole | | 97% | 1.83 cm²/V·s | **749257-500MG** |
| 5,5′′′-Bis(tridecafluorohexyl)-2,2′:5′,2′′:5′′,2′′′-quaterthiophene | | - | ≤0.64 cm²/V·s | **764639-250MG**<br>**764639-1G** |
| 2,7-Dihexylbenzo[lmn][3,8]phenanthroline-1,3,6,8(2H,7H)-tetrone | | ≥97.6% | 0.7 cm²/V·s | **768464-500MG** |
| 1,3,6,8(2H,7H)-Tetraone, 2,7-dicyclohexylbenzo[lmn][3,8] phenanthroline | | 98% | 6 cm²/V·s | **761443-1G** |
| N,N′-Dimethyl-3,4,9,10-perylenedicarboximide | | 98% | $10^{-5}$ cm²/V·s | **771481-1G**<br>**771481-5G** |
| 2,9-Dipropylanthra[2,1,9-def:6,5,10-d′e′f′]diisoquinoline-1,3,8,10(2H,9H)tetrone | | 97% | 0.1-2.1 cm²/V·s | **771635-1G** |
| N,N′-Dipentyl-3,4,9,10-perylenedicarboximide | | 98% | ~$10^{-4}$ cm²/V·s | **663921-500MG** |
| 2,9-Dihexylanthra[2,1,9-def:6,5,10-d′e′f′]diisoquinoline-1,3,8,10(2H,9H)tetrone | | 98% | 0.1-2.1 cm²/V·s | **773816-1G** |
| 2,9-Diheptylanthra[2,1,9-def:6,5,10-d′e′f′]diisoquinoline-1,3,8,10(2H,9H)tetrone | | 99% | $1.4\times10^{-2}$ cm²/V·s | **773824-1G** |

| Name | Structure | Purity | Mobility | Cat. No. |
|---|---|---|---|---|
| N,N'-Dioctyl-3,4,9,10-perylenedicarboximide | | 98% | 1.7 cm²/V·s | **663913-1G** |
| N,N'-Diphenyl-3,4,9,10-perylenedicarboximide | | 98% | $10^{-5}$ cm²/V·s | **663905-500MG** |
| N,N'-Bis(2,5-di-tert-butylphenyl)-3,4,9,10-perylenedicarboximide | | 97% | $1.8 \times 10^{-4}$ cm²/V·s | **264229-100MG** |
| 2,9-Bis[(4-methoxyphenyl)methyl]anthra[2,1,9-def:6,5,10-d'e'f']diisoquinoline-1,3,8,10(2H,9H)tetrone | | 99% | 0.5 cm²/V·s | **771627-1G** |
| 1,3,8,10(2H,9H)-Tetraone, 2,9-bis(2-phenylethyl)anthra[2,1,9-def:6,5,10-d'e'f']diisoquinoline | | 98%, elemental analysis | 1.4 cm²/V·s | **761451-1G** |
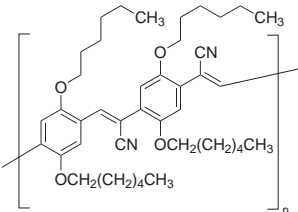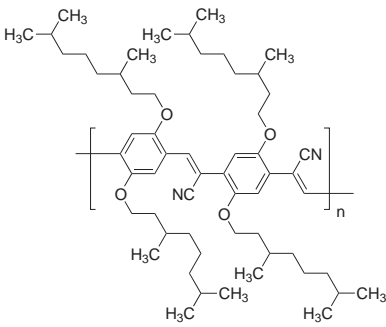
## N-type Polymers

For a complete list of available materials, visit **SigmaAldrich.com/npoly**.

| Name | Structure | Mobility | Cat. No. |
|---|---|---|---|
| Poly(benzimidazobenzophenanthroline) | | 0.1 cm²/V·s<br>0.4 cm²/V·s | **667846-250MG**<br>**667846-1G** |
| Poly(5-(3,7-dimethyloctyloxy)-2-methoxy-cyanoterephthalylidene) | | $\sim 10^{-5}$ cm²/V·s | **646628-250MG** |
| Poly(5-(2-ethylhexyloxy)-2-methoxy-cyanoterephthalylidene) | | $\sim 10^{-5}$ cm²/V·s | **646644-250MG** |

| Name | Structure | Mobility | Cat. No. |
|---|---|---|---|
| Poly(2,5-di(hexyloxy)cyanoterephthalylidene) |  | ~$10^{-5}$ cm²/V·s | **646652-250MG** |
| Poly(2,5-di(3,7-dimethyloctyloxy) cyanoterephthalylidene) |  | ~$10^{-5}$ cm²/V·s | **646571-250MG** |

# Organic Optoelectronics on Shape Memory Polymers

Canek Fuentes-Hernandez, Bernard Kippelen*

Center for Organic Photonics and Electronics (COPE), School of Electrical and Computer Engineering, Georgia Institute of Technology, Atlanta, Georgia 30332, USA
*E-mail: bernard.kippelen@ece.gatech.edu

## Introduction

The drive toward device integration over the past 50 years has produced a staggering miniaturization of integrated circuits and increased computing power. In the age of mobile computing, a pocket-size smartphone contains a processor with billions of transistors, has a display and a camera with millions of pixels, and is capable of performing billions of calculations per second, even more computing power than IBM's Deep Blue, the most powerful supercomputer in the world in 1996. Along with the internet, mobile computing has produced an information revolution over the last decade that has renewed interest in the development of lightweight, flexible, and stretchable electronics for wearable devices, robotics, and autonomous vehicles, helping to realize the vision of ubiquitous computing and the internet of things. In the same period of time, new technologies for the control of biological processes have revolutionized biological and medical sciences, creating an urgent need for stretchable soft electronics that bridge the gap between the biological world and that of stiff optoelectronic technologies. In this context, the new generation of stretchable semiconductors, elastic substrates, and optoelectronic device architectures are poised to provide form-factors and functionalities (i.e. sensing, power generation and storage, wireless communication) that are complementary to those provided by the enormous computing power of mobile devices. When combined, these technologies offer the potential to dramatically change the ways in which humans experience and interact with the natural and the digital world. Here, we provide a short review of advances in the area of soft optoelectronics, with a focus on the development of organic optoelectronic devices on shape memory polymers (SMP).

## The Emergence of Soft Optoelectronics

Interest in soft materials for optoelectronics has seen a dramatic increase in recent years, with impressive demonstrations of lightweight ultraflexible and stretchable devices such as thin-film transistors, photovoltaics, imaging arrays, light-emitting diodes, and many others.[1] Despite great progress, these efforts also highlight the need for further innovations in semiconducting and elastic materials as well as in novel device architectures.

From a material perspective, novel materials must be engineered to display thermomechanical properties that better match those found in natural biological materials, such as cellular materials, elastomers, polymers and polymer composites, and ceramics. At the same time, these novel materials must preserve the optical and electrical properties required to ensure their functionality in device architectures. To understand these requirements, we must consider that in general, biological materials have a low density ($<3$ g/cm$^3$) with a Young's modulus that can vary in the range from kPa to ca. 100 GPa, while their (yield/fracture) strength varies in the range from tens of kPa up to a few GPa, depending on the type of material.[2] For instance, natural elastomers such as skin, muscles, and arteries display a Young's modulus smaller than 80 MPa and strength smaller than 10 MPa.[2] These mechanical properties are in sharp contrast with those displayed by traditional stiff optoelectronic devices comprised of rigid materials like metals, metal-oxides, and inorganic semiconductors. This is because inorganic materials have a density in the range from 2 to 20 g/cm$^3$, a Young's modulus in the range from 10 to 1,000 GPa and a strength in the range from 8 to 2000 MPa.[3,4] Furthermore, these materials generally require high degrees of crystallinity to enable efficient charge transport and consequently are processed at high temperatures that are typically incompatible with soft biological substrates.

Despite challenges, rigid materials have been engineered to enable flexible and even stretchable optoelectronic devices. To understand this, it is important to note that the flexibility of a thin plate of a rigid material, quantified as the flexural rigidity $D$, depends cubically on the film's thickness, is proportional to the Young's modulus, and inversely proportional to one minus the square of the Poisson's ratio of the material (i.e. the ratio of transverse contraction strain to longitudinal extension strain in the direction of the stretching force, typically in the range from 0.1, for stiff materials, to 0.5 for soft materials).[5] Consequently, films of rigid materials with a large Young's modulus in the hundreds of GPa range (e.g. glass, metals, silicon, metal-oxides, etc.) can become relatively flexible if processed into sufficiently thin films with a typical thickness of tens to hundreds of nanometers.[4]

Although optoelectronic devices comprised of thin films of rigid materials can be flexible, they are generally not very stretchable. To generate stretchable devices out of rigid materials, three main approaches shown in **Figure 1** have been explored. In the first approach, small discrete devices deposited or transferred onto an elastomer substrate are connected with stretchable wirings. In the second and more common approach, flexible functional devices are fabricated or laminated onto a pre-stretched elastomer substrate, which is allowed to wrinkle when the strain is released. This strategy has been used to generate stretchable optoelectronic devices, comprising rigid materials, on soft elastic substrates such as poly(dimethylsiloxane) (PDMS).[1,6] On the other hand, the emergence of nanostructured materials such as nanoparticles and nanowires has provided another route towards the realization of flexible and stretchable devices. In this approach, percolating networks of nanomaterials such as Ag nanowires (Cat. Nos. **778095, 739421** and **739448**) are embedded in an elastomer matrix such as PDMS, by mixing nanomaterials and elastomer monomers prior to curing.[7] Furthermore, stretchable sensors have also been fabricated using eutectic metal alloys (eutectic gallium–indium alloy, EuGaIn that is liquid at room temperature, **Cat. No. 495425**) embedded in PDMS using soft lithography and may provide an attractive route towards developing fully stretchable electrodes.[8]
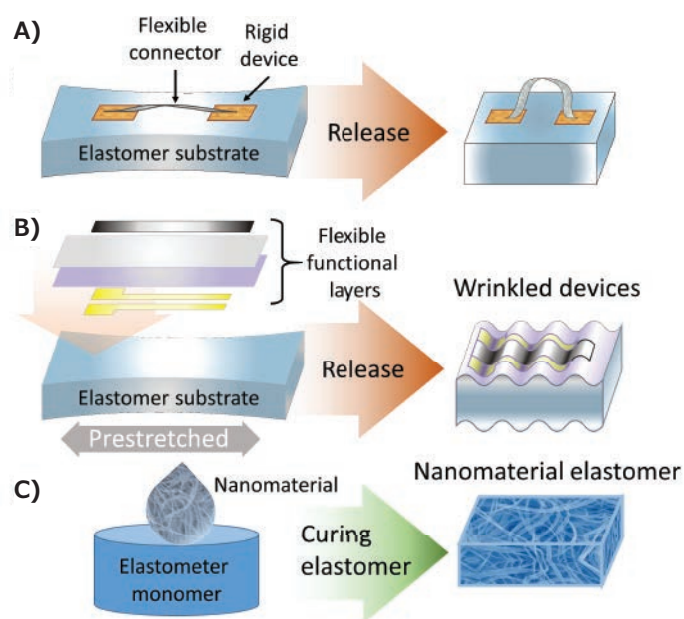


**Figure 1.** Approaches towards stretchable optoelectronics. **A**) Discrete devices are connected with each other using stretchable wirings. **B**) Stretchable devices are fabricated by depositing the flexible layers of a device onto a pre-stretched elastomer (elastic) substrate, resulting in wrinkled devices upon releasing the strain on the substrate. **C**) Nanomaterials mixed with elastomer monomer followed by curing.

## Organic Optoelectronics

In contrast to inorganic semiconductors, organic semiconductors display thermomechanical properties (e.g. low density below 3 g/cm^{3} and Young's modulus in the range 0.1 to 1 GPa)[9] that are better matched to those of soft biological materials. In addition, organic semiconductor films are processed from solution at temperatures that are compatible with a wide range of soft elastic substrates. Consequently, the use of organic semiconductor films (polymers, small molecules, or blends) has led to the realization of ultra-flexible optoelectronic devices, such as thin-film transistors and photovoltaics[10,11] that remain operational when flexed to a bending radius down to a few microns. Despite their inherent flexibility, the stretchability of organic semiconductors largely depends on their molecular weight, molecular packing in the solid state, and their molecular composition.[9,12-14] Generally, amorphous polymer films display superior mechanical properties (i.e. smaller Young's modulus), including stretchability, but also display inferior charge transport properties than films comprising more rigid materials such as crystalline polymers or small molecules.[12] Because of this tradeoff, stretchable organic optoelectronic devices have largely relied on similar approaches to those used for inorganic semiconductors; fabrication of wrinkled devices on pre-stretched substrates or use of nanomaterials, such as carbon nanotubes, embedded on an elastic matrix.[15] However, the ability to tailor the properties of organic semiconductors using synthetic chemistry and compositional engineering has, in recent years, produced important advances towards developing truly stretchable organic semiconductor layers. In one approach, polymer semiconductor nanofibers of high-mobility semiconducting polymers were formed through phase separation inside a soft elastic matrix (polystyrene-*b*-poly(ethylene-ran-butylene)-*b*-polystyrene (SEBS), **Cat. Nos. 200565** and **200557**) leading to the devlopment of highly stretchable polymer semiconductor films and stretchable thin-film transistors that display charge mobility values in the range between 0.5 to 1 cm$^2$/Vs even when subjected to a strain of 100%.[16] In the second approach, akin to the connection of devices with stretchable wirings, molecular stretchability is engineered into conjugated polymers by adding chemical moieties to the backbone that, on one hand, do not hinder the formation of crystalline domains and, on the other, promote dynamic non-covalent crosslinking between flexible polymer chains in the amorphous regions. These dynamic bonds can easily break upon strain to dissipate energy through the amorphous regions while preserving the integrity of charge transport through the more ordered regions.[14] Following this approach, semiconductor polymer films and thin-film transistors can be stretched up to 100% strain while displaying charge mobility values ca. 1 cm$^2$/Vs.[14] In addition to achieving high stretchability, this approach could also enable self-healing properties.[14]

Continued progress in the development of novel materials, material processing, and device engineering is producing significant advances in the performance and stability of organic-base optoelectronics devices such as organic thin-film transistors (OTFTs), organic light-emitting diodes (OLED), and organic photovoltaics (OPV). Reviewing the extensive amount of progress in each area is out of the scope of this contribution.

## Soft Elastic Substrates

An integral component of any stretchable optoelectronic device is the selection of the elastic substrate. Elastic substrates must display characteristics such as (1) a Young's modulus approaching that of the targeted biological material (e.g. Young's modulus of the skin is ca. 0.7 MPa), (2) a low Poisson's ratio to avoid the formation of cracks, (3) good thermomechanical stability to ensure repeatable deformation, (4) chemical stability and biocompatibility to allow the direct fabrication of optoelectronic devices, and (5) compatibility with the targeted biological materials. To date, PDMS remains the most widely used elastic substrate for stretchable devices. PDMS offers excellent stability and biocompatibility, but its stretchability is typically limited to 200%. Alternative materials that can achieve stretchability of ca. 700% are Ecoflex, a platinum-catalyzed silicone17 and poly[styrene-*b*-(ethylene-*co*-butylene)-*b*-styrene] resin and 3M™ VHB™ 4905 (transparent tape with a general-purpose acrylic adhesive).[18] Other elastic substrates include polyurethanes and polyacrylate elastomers.[6]

## Shape-memory Polymers

Among the wide range of potential soft substrates, shape-memory polymers (SMPs) are an emerging class of active stimuli-responsive polymers with many properties that are attractive to the development of biomedical, robotic, and autonomous vehicle applications. SMPs display the ability of changing their shape in response to external stimuli. When this stimulus is temperature, SMPs are thermoresponsive. A thermoresponsive SMP presents three temperature-dependent states, a glassy state at low temperature characterized by a large Young's modulus and low deformability. A region at a higher temperature where the material softens and exhibits pseudoelastic properties. This region is characterized by the glass transition temperature, $T_g$, around which the Young's modulus experiences a drastic drop in value. At temperatures higher than $T_g$, the SMP enters into the rubbery regime, characterized by a small Young's modulus and high deformability. In this region, the shape of the SMP can be modified and the modified shape can be preserved (or maintained) if the temperature is reduced below $T_g$. If the SMP is once more reheated above $T_g$, the transition into the rubbery regime causes the SMP to regain its original shape. To understand this reshaping mechanism, we need to consider that polymer networks in an SMP form in a stress-free, global, free-energy minimum that minimizes the entropy of the system. Upon heating, deformation, and cooling, configurational changes in the polymer chains acquire and store mechanical stress in the polymer, creating a higher-entropy stressed metastable equilibrium, which upon heating and in the absence of further mechanical deformations, relaxes back into the lower entropy, stress-free state characterized by the original polymer shape. This process is illustrated in **Figure 2**, where the SMP has been casted on a curved mold. The ability of an SMP to recover its shape is quantified as the recoverable strain. This ability to control the rigidity and shape of SMP substrates consequently could offer potential advantages over elastic substrates for the fabrication, handling, and deployment of soft optoelectronic devices.



As casted, curved SMPs    Crumpled after heating    Heating the crumpled SMPs in water    Self-recover the initial shape

$T_g$ of SMPs = 43 °C, $T_{water}$ = 60 °C
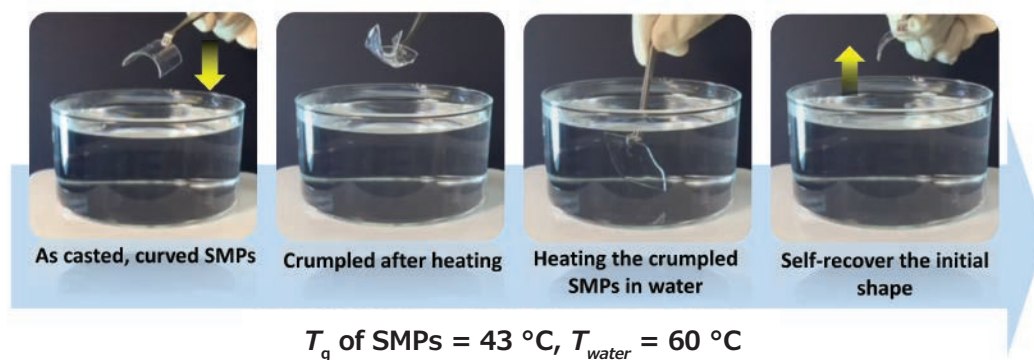
**Figure 2.** Shape recovery of curved SMP.

## Organic Electronics on Shape Memory Polymers

Recently, thiolene chemistries have yielded SMPs that are biocompatible[19–21] and suitable for use as active substrates for mechanically adaptable OTFTs.[22-26] SMPs based on thiolene reactions (click reactions) display low-cure stresses due to the nature of the step-growth mechanism in this polymerization, resulting in highly uniform/dimensionally stable polymer networks with low shrinkage and surface roughness, as well as strong adhesion to metal layers. More significantly, this allows for various material properties (such as $T_g$, rubbery modulus, and hydrophobicity) to be altered by controlling the concentration of the constituting monomers. For example, varying the concentration of tricyclo[5.2.1.0$^{2,6}$]decanedimethanol diacrylate (TCMDA, **Cat. No. 496669**) in a blend of 1,3,5-triallyl-1,3,5-triazine-2,4,6(1*H*,3*H*,5*H*)-trione (TATATO, **Cat. No. 114235**), trimethylolpropane tris(3-mercaptopropionate) (TMTMP, **Cat. No. 381489**), and 2,2-dimethoxy-2-phenyl acetophenone (DMPA, **Cat. No. 196118**), a photocuring agent, changes the $T_g$ of the SMP. We have recently taken this SMP composition to explore the realization of top-gate OTFTs with bilayer gate dielectrics and OLEDs.
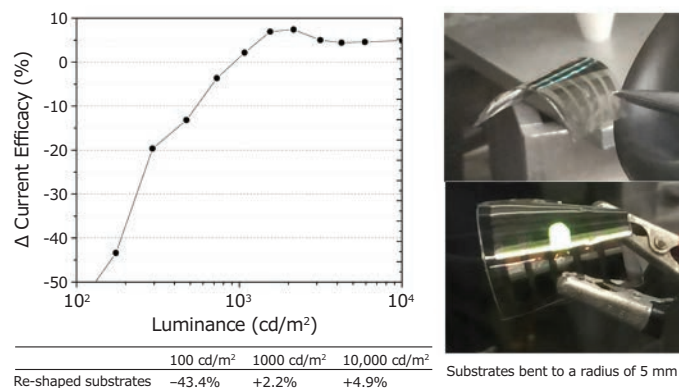
In the past, we have shown n- and p-channel top-gate OTFTs can be engineered to display excellent operational and environmental stability when a bilayer gate dielectric comprising a first CYTOP layer and a second metal-oxide layer processed by atomic layer deposition (ALD) is used.[27,28] In this approach, the bilayer gate dielectric serves the role of an environmental barrier and introduces a second mechanism (e.g. dipolar orientation or charge injection) to compensate the threshold voltage shift induced by charge trapping. This device geometry produces OTFTs that sustain immersion in water for prolonged periods of time at temperatures near its boiling point,[29] opening the door for stable chemical and biological sensors that operate in aqueous conditions.[30,31] In addition, we have investigated the properties of top-gate OTFTs and circuits on thiolene based SMP substrates[32] designed to yield a $T_g$ of 43 °C. **Figure 3**, shows the properties of single devices and pseudo-complementary inverter circuits comprising solution-processed OTFTs, with a bilayer comprising a 35 nm layer of CYTOP and a 31 nm-thick dielectric nanolaminate[29] fabricated by ALD on ca. 130 μm-thick SMP substrates. Compared to single-material ALD layers, the use of a nanolaminate was found to yield reduced cracking under mechanical deformation, possibly due to a reduction in the residual tensile stress produced during the ALD layers.[33] OTFTs on SMPs yield mobility values of 0.9 ± 0.59 cm$^2$/Vs with very small contact resistance due to the deposition of the p-type dopant molybdenum

tris[1,2-bis(trifluoromethyl)ethane-1,2-dithiolene] (Mo(tfd)3 **Cat. No. 795712**)[34–37] onto the source and drain electrodes. This level of performance is comparable to that displayed by top-gate OTFTs on glass or plastic substrates. In addition, devices exhibit good flexibility at room temperature, with no changes of their transfer characteristic before and after undergoing a compressive bending cycle down to a 7 mm radius of curvature (strain ca. 0.9%). When OTFTs are subjected to thermally-induced reshaping, devices maintain a high level of performance down to a bending radius of ca. 14 mm. However, beyond this point, the performance deteriorates due to cracking of the ALD nanolaminate layer, suggesting that the device is presumably subjected to large strains during the reshaping process. It should be noted that typical polycrystalline organic semiconducting layers[9,12] as well as ALD layers[38] are known to undergo significant cracking or even failure when reaching critical tensile strains in the range from ca. 1-2%. While the use of ALD layers may impose limitations to the development of fully stretchable devices, the benefits in device performance and stability may offset such limitations in applications that may not require extreme deformations. Alternatively, fabrication of OTFTs on pre-stretched SMPs may offer an alternative path towards improving the mechanical resilience of environmentally and operationally stable OTFTs.
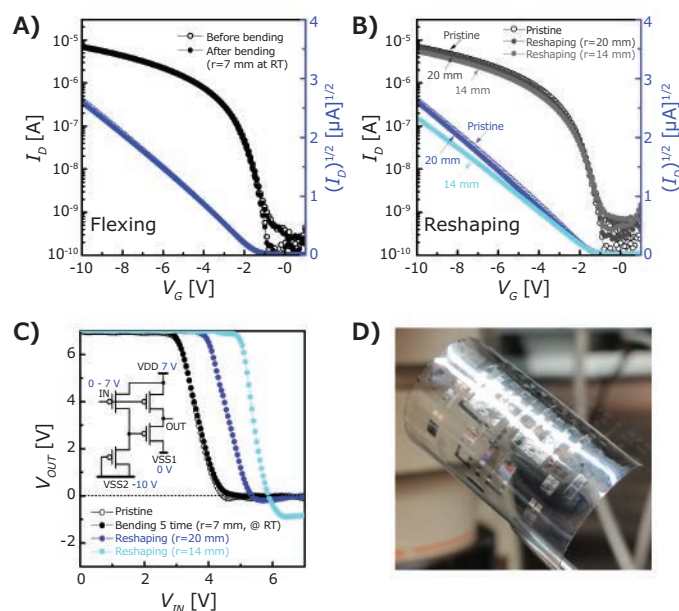


**Figure 3.** A) Transfer characteristics of OTFTs on SMPs before and after flexing. B) Transfer characteristics of OTFTs on SMPs before and after thermally-induced reshaping at 60 °C. C) Output characteristics of pseudo-complementary inverted before and after thermally-induced reshaping. D) Photograph of curved pseudo-complementary inverter circuits on SMPs.

It should be noted that while other design strategies exist for improving the environmental stability of OTFTs through the passivation of defects using molecular additives such as 7,7,8,8-Tetracyanoquinodimethane (TCNQ, **Cat. No. 157635**), 2,3,5,6-Tetrafluoro-7,7,8,8-tetracyanoquinodimethane (F4TCNQ, **Cat. No. 376779**) and 4-aminobenzonitrile (ABN),[39] improved design strategies will be needed for the development of stretchable OTFTs that display both high operational and environmental stability at the same time.



| | 100 cd/m² | 1000 cd/m² | 10,000 cd/m² |
|---|---|---|---|
| Re-shaped substrates | −43.4% | +2.2% | +4.9% |

Substrates bent to a radius of 5 mm

**Figure 4.** Change in current efficacy of OLED on SMPs after reshaping and images of devices under tensile strength.

On the other hand, OLEDs also offer important opportunities to develop large-area light sources with low heat dissipation, attractive characteristics for optogenetic and other bioengineering applications, particularly when fabricated on biocompatible SMPs. OLEDs on SMP substrates were first demonstrated using a single-walled carbon nanotube/polymer composite electrode as an indium tin oxide (ITO) replacement. These devices produced a maximum current efficacy of 1.24 cd/A at 200 cd/m² with a turn-on voltage of 4.8 V, and a maximum luminance of 300 cd/m². More recently, we reported the development of inverted top-emitting green-phosphorescent OLEDs fabricated on biocompatible SMP substrates that produced current efficiencies of 33 cd/A at a high luminance of 1,000 cd/m² with a low turn-on voltage of 3.4 V. These devices produce a maximum luminance of over 30,000 cd/m², making them ideal candidates for bioengineering applications that require high irradiance levels.[40] Moreover, these samples can be re-shaped and softened into a curved form factor with a bending radius of 5 mm (strain ca. 1.5%). Although these devices show a significant performance drop at low luminance levels (100 cd/m²), they perform equally as well when larger biases are applied and show great promise for applications that require high luminance values (**Figure 4**). All the devices measured could withstand the initial heating, reshaping, and return to their original form factors. Further opportunities to improve the performance and thermomechanical properties of OLEDs on biocompatible SMPs may exist with the use of thermally-activated delayed fluorescence (TADF) chromophores[41] and high-$T_g$ electron and hole transport materials.[42] These tests demonstrate the ability to thermally evaporate inverted top-emitting OLEDs on SMP substrates for flexible and conformable devices, highlighting the potential for such sources for a variety of applications. However, the mechanical properties of these evaporated OLEDs are still limited and can lead to cracking of the metal layers and ultimately failure of the OLEDs upon repeated reshaping or under more severe deformation. Detailed studies are needed to assess the sources of failure and to address the best way to ensure the mechanical reliability of OLEDs on SMPs.

## Conclusions and Outlook

To reach the full potential of organic optoelectronics on soft substrates such as SMP's, several problems still need to be addressed. One of the most pressing needs is ensuring adequate environmental and operational stability of devices fabricated on soft substrates. Environmental barriers such as those deposited by ALD on soft elastic substrates should be investigated to develop an in-depth understanding of the potential of using rigid barrier layers meant to improve environmental stability and reduce constraints pertaining to moisture penetration. From a material perspective, great progress has been made in developing organic semiconductors with stabilized frontier orbitals that are less prone to oxidation.[30,43-45] Confinement of charge transport in nanoaggregates also appears to be a promising avenue for developing materials that are at the same time stretchable and may be less prone to interactions with oxygen and water in the environment. In addition, molecular additives have recently been demonstrated to improve the stability of OLEDs,[46] OTFTs,[39] and OPVs.[47] On the other hand, advances in interfacial engineering show work function engineering is an effective route to improve the stability of devices. As an example, we have found that polyethylenimine ethoxylated (PEIE, **Cat. No. 306185**) and branched polyethylenimine (PEI, **Cat. No. 482595**)[48] not only enable efficient electron injection and collection from a wide range of environmentally stable conductors, but this approach has also been shown to improve OPV stability.[49] Aside from reducing the work function, these materials also lead to n-doping of organic semiconductors[48] and consequently open the door for the creation of n-doped regions by phase segregation, shown to produce self-assembled electron-collecting interfaces in OPV devices.[50] Analogously, the use of p-dopants is expected to provide a path towards creating environmentally robust interfaces that avoid use of reactive metals and also may lead to simplification of a device architecture. For example, we recently discovered organic semiconductor films are efficiently p-doped to a limited-depth by post-process immersion in a solution of phosphomolybdic acid (PMA, **Cat. No. 431400**) in nitromethane (**Cat. No. 360554**). The ability to electrically dope the interface removes constraints on the work function of the metal used, and when applied to a bulk-heterojunction film in which PEIE was mixed in solution prior to film formation, enables the realization

of single-layer OPVs in which the electron-collection and hole-collection functionalities are embedded within the photoactive layer.[51] Hence, although the development of stretchable organic semiconductors and devices architectures may still be at its infancy, advances in the area of organic optoelectronics can be expected to enable the realization of devices that are not only mechanically compliant but that also achieve the level of performance required for next generation stretchable optoelectronic devices.

## Acknowledgements

## References

(1) Bauer, S.; Bauer-Gogonea, S.; Graz, I.; Kaltenbrunner, M.; Keplinger, C.; Schwödiauer, R. *Adv. Mater.* **2014**, *26*, 149–162.

(2) Meyers, M. A.; Chen, P.-Y.; Lin, A. Y.-M.; Seki, Y. *Prog. Mater. Sci.* **2008**, *53*, 1–206.

(3) Fleck, N. A.; Deshpande, V. S.; Ashby, M. F. *Proc. Royal Soc. A* **2010**, DOI: 10.1098/rspa.2010.0215.

(4) McCoul, D.; Hu, W.; Gao, M.; Mehta, V.; Pei, Q. *Adv. Electron. Mater.* **2016**, *2*, 1500407.

(5) Greaves, G. N.; Greer, A. L.; Lakes, R. S.; Rouxel, T. *Nat. Mater.* **2011**, *10*, 986–986.

(6) Qi, D.; Liu, Z.; Leow, W. R.; Chen, X. *MRS Bull.* **2017**, *42*, 103–107.

(7) Xu, F.; Zhu, Y. *Adv. Mater.* **2012**, *24*, 5117–5122.

(8) Kim, M.-G.; Alrowais, H; Pavlidis, S.; Brand, O. *Adv. Funct. Mater.* **2017**, *27*, 1604466.

(9) Roth, B.; Savagatrup, S.; de los Santos, N. V.; Hagemann, O.; Carlé, J. E.; Helgesen, M.; Livi, F.; Bundgaard, E.; Søndergaard, R. R.; Krebs, F. C.; Lipomi, D. J. *Chem. Mater.* **2016**, *28*, 2363–2373.

(10) Yi, H. T.; Payne, M. M.; Anthony, J. E.; Podzorov, V. *Nat. Commun.* **2012**, *3*, 1259.

(11) Someya, T.; Bauer, S.; Kaltenbrunner, M. *MRS Bull.* **2017**, *42*, 124–130.

(12) Onorato, J.; Pakhnyuk, V.; Luscombe, C. K. *Polym. J.* **2017**, *49*, 41–60.

(13) Xu, J.; Wang, S.; Wang, G.-J. N.; Zhu, C.; Luo, S.; Jin, L.; Gu, X.; Chen, S.; Feig, V. R.; To, J. W. F.; Rondeau-Gagné, S.; Park, J.; Schroeder, B. C.; Lu, C.; Oh, J. Y.; Wang, Y.; Kim, Y.-H.; Yan, H.; Sinclair, R.; Zhou, D.; Xue, G.; Murmann, B.; Linder, C.; Cai, W.; Tok, J. B.-H.; Chung, J. W.; Bao, Z. *Science* **2017**, *355*, 59–64.

(14) Oh, J. Y.; Rondeau-Gagné, S.; Chiu, Y.-C.; Chortos, A.; Lissel, F.; Wang, G.-J. N.; Schroeder, B. C.; Kurosawa, T.; Lopez, J.; Katsumata, T.; Xu, J.; Zhu, C.; Gu, X.; Bae, W.-G.; Kim, Y.; Jin, L.; Chung, J. W.; Tok, J. B. H.; Bao, Z. *Nature* **2016**, *539*, 411–415.

(15) Lipomi, D. J.; Vosgueritchian, M.; Tee, B. C. K.; Hellstrom, S. L.; Lee, J. A.; Fox, C. H.; Bao, Z. *Nat. Nanotechnol.* **2011**, *6*, 788–792.

(16) Xu, J.; Wang, S.; Wang, G.-J. N.; Zhu, C.; Luo, S.; Jin, L.; Gu, X.; Chen, S.; Feig, V. R.; To, J. W. *Science* **2017**, *355*, 59–64.

(17) Cai, G.; Wang, J.; Qian, K.; Chen, J.; Li, S.; Lee, P. S. *Adv. Sci.* **2016**, DOI: 10.1002/advs.201600190.

(18) Zhu, S.; So, J.-H.; Mays, R.; Desai, S.; Barnes, W. R.; Pourdeyhimi, B.; Dickey, M. D. *Adv. Funct. Mater.* **2013**, *23*, 2308–2314.

(19) Ware, T.; Simon, D.; Arreaga-Salas, D. E.; Reeder, J.; Rennaker, R.; Keefer, E. W.; Voit, W. *Adv. Funct. Mater.* **2012**, *22*, 3470–3479.

(20) Mather, P. T.; Luo, X.; Rousseau, I. A. *Annu. Rev. Mater.* **2009**, *39*, 445–471.

(21) Meng, H.; Li, G. *Polymer* **2013**, *54*(9), 2199–2221.

(22) Liu, Y.; Boyles, J. K.; Genzer, J.; Dickey, M. D. *Soft Matter* **2012**, *8*, 1764–1769.

(23) Wang, H.; Wang, Y.; Tee, B. C. K.; Kim, K.; Lopez, J.; Cai, W.; Bao, Z. *Adv. Sci.* **2015**, DOI: 10.1002/advs.201500103.

(24) Avendano-Bolivar, A.; Ware, T.; Arreaga-Salas, D.; Simon, D.; Voit, W. *Adv. Mater.* **2013**, *25*, 3095–3099.

(25) Reeder, J.; Kaltenbrunner, M.; Ware, T.; Arreaga-Salas, D.; Avendano-Bolivar, A.; Yokota, T.; Inoue, Y.; Sekino, M.; Voit, W.; Sekitani, T.; Someya, T. *Adv. Mater.* **2014**, *26*, 4967–4973.

(26) Lu, H.; Liang, F.; Yao, Y.; Gou, J.; Hui, D. *Compos. Part B-Eng.* **2014**, *59*, 191–195.

(27) Hwang, D. K.; Dasari, R. R.; Fenoll, M.; Alain-Rizzo, V.; Dindar, A.; Shim, J. W.; Deb, N.; Fuentes-Hernandez, C.; Barlow, S.; Bucknall, D. G.; Audebert, P.; Marder, S. R.; Kippelen, B. *Adv. Mater.* **2012**, *24*, 4445–4450.

(28) Hwang, D. K.; Fuentes-Hernandez, C.; Fenoll, M.; Yun, M.; Park, J.; Shim, J. W.; Knauer, K.; Dindar, A.; Kim, H.; Kim, Y. *ACS Appl. Mater. Inter.* **2014**, *6*, 3378–3386.

(29) Wang, C.-Y.; Fuentes-Hernandez, C.; Yun, M.; Singh, A.; Dindar, A.; Choi, S.; Graham, S.; Kippelen, B. *ACS Appl. Mater. Inter.* **2016**, *8*, 29872–29876.

(30) Roberts, M. E.; Mannsfeld, S. C. B.; Queralto, N.; Reese, C.; Locklin, J.; Knoll, W.; Bao, Z. *Proc. Natl. Acad. Sci. U.S.A.* **2008**, *105*, 12134–12139.

(31) Yun, M.; Sharma, A.; Fuentes-Hernandez, C.; Hwang, D. K.; Dindar, A.; Singh, S.; Choi, S.; Kippelen, B. *ACS Appl. Mater. Inter.* **2014**, *6*, 1616–1622.

(32) Choi, S.; Fuentes-Hemandez, C.; Wang, C.-Y.; Wei, A.; Voit, W.; Zhang, Y.; Barlow, S.; Marder, S. R.; Kippelen, B. *SPIE Organic Photonics Electronics* **2015**, 95680A-95680A-5.

(33) Bulusu, A.; Singh, A.; Wang, C.; Dindar, A.; Fuentes-Hernandez, C.; Kim, H.; Cullen, D.; Kippelen, B.; Graham, S. *J. Appl. Phys.* **2015**, *118*, 085501.

(34) Davison, A.; Holm, R. H.; Benson, R. E.; Mahler, W. *Inorg. Synth.* **1967**, *10*, 8–26.

(35) Qi, Y.; Sajoto, T.; Barlow, S.; Kim, E.-G.; Brédas, J.-L.; Marder, S. R.; Kahn, A. *J. Am. Chem. Soc.* **2009**, *131*, 12530–12531.

(36) Tiwari, S. P.; Potscavage Jr, W. J.; Sajoto, T.; Barlow, S.; Marder, S. R.; Kippelen, B. *Org. Electron.* **2010**, *11*, 860–863.

(37) Choi, S.; Fuentes-Hernandez, C.; Wang, C.-Y.; Khan, T. M.; Larrain, F. A.; Zhang, Y.; Barlow, S.; Marder, S. R.; Kippelen, B. *ACS Appl. Mater. Inter.* **2016**, *8*, 24744–24752.

(38) Jen, S.-H.; Bertrand, J. A.; George, S. M. *J. Appl. Phys.* **2011**, *109*, 084305.

(39) Nikolka, M.; Nasrallah, I.; Rose, B.; Ravva, M. K.; Broch, K.; Sadhanala, A.; Harkin, D.; Charmet, J.; Hurhangee, M.; Brown, A.; Illig, S.; Too, P.; Jongman, J.; McCulloch, I.; Bredas, J.-L.; Sirringhaus, H. *Nat Mater.* **2016**, *16*, 356–362.

(40) Gaj, M. P.; Wei, A.; Fuentes-Hernandez, C.; Zhang, Y.; Reit, R.; Voit, W.; Marder, S. R.; Kippelen, B. *Org. Electron.* **2015**, *25*, 151–155.

(41) Uoyama, H.; Goushi, K.; Shizu, K.; Nomura, H.; Adachi, C. *Nature* **2012**, *492*, 234–238.

(42) Gaj, M. P.; Fuentes-Hernandez, C.; Zhang, Y.; Marder, S. R.; Kippelen, B. *Org. Electron.* **2015**, *16*, 109–112.

(43) Hwang do, K.; Dasari, R. R.; Fenoll, M.; Alain-Rizzo, V.; Dindar, A.; Shim, J. W.; Deb, N.; Fuentes-Hernandez, C.; Barlow, S.; Bucknall, D. G.; Audebert, P.; Marder, S. R.; Kippelen, B. *Adv Mater.* **2012**, *24*, 4445–4450.

(44) Knopfmacher, O.; Hammock, M. L.; Appleton, A. L.; Schwartz, G.; Mei, J.; Lei, T.; Pei, J.; Bao, Z. *Nat. Commun.* **2014**, *5*, 2954.

(45) Sirringhaus, H. *Adv. Mater.* **2014**, *26*, 1319–1335.

(46) Tsang, D. P.-K.; Matsushima, T.; Adachi, C. *Sci. Rep.* **2016**, *6*, 22463.

(47) Shang, Z.; Heumueller, T.; Prasanna, R.; Burkhard, G. F.; Naab, B. D.; Bao, Z.; McGehee, M. D.; Salleo, A. *Adv. Energy Mater.* **2016**, *6*, 1601149.

(48) Zhou, Y.; Fuentes-Hernandez, C.; Shim, J.; Meyer, J.; Giordano, A. J.; Li, H.; Winget, P.; Papadopoulos, T.; Cheun, H.; Kim, J.; Fenoll, M.; Dindar, A.; Haske, W.; Najafabadi, E.; Khan, T. M.; Sojoudi, H.; Barlow, S.; Graham, S.; Brédas, J.-L.; Marder, S. R.; Kahn, A.; Kippelen, B. *Science* **2012**, *336*, 327–332.

(49) Weerasinghe, H. C.; Rolston, N.; Vak, D.; Scully, A. D.; Dauskardt, R. H. *Sol. Energy Mater. Sol. Cells* **2016**, *152*, 133–140.

(50) Kang, H.; Lee, J.; Jung, S.; Yu, K.; Kwon, S.; Hong, S.; Kee, S.; Lee, S.; Kim, D.; Lee, K. *Nanoscale* **2013**, *5*, 11587–11591.

(51) Kolesov, V. A.; Fuentes-Hernandez, C.; Chou, W.-F.; Aizawa, N.; Larrain, F. A.; Wang, M.; Perrotta, A.; Choi, S.; Graham, S.; Bazan, G. C.; Nguyen, T.-Q.; Marder, S. R.; Kippelen, B. *Nat. Mater.* **2016**, DOI: 10.1038/NMAT4818.
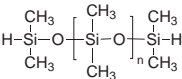
## Polydimethylsiloxane (PDMS)

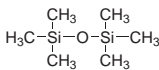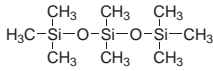For a complete list of available materials, visit **SigmaAldrich.com/pdms**.
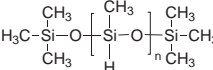
### SYLGARD® Silicone

| Name | Description | Size | Cat. No. |
|---|---|---|---|
| SYLGARD® 184 | Preweighed monomer and curing agent in convenient blister packs. | 10 g clip-pack | **761036-5EA** |
| | | 5 g clip-pack | **761028-5EA** |
| | SYLGARD 184 Silicone Elastomer Kit is comprised of Base/Curing Agent to be mixed in a 10 (base) :1 (curing agent) ratio by weight for manual mixing. | | |
| SYLGARD® 170 silicone elastomer | Form: Black liquid (part A), off-white liquid (part B) Viscosity: 3160 cPs (part A), 1110 cPs (part B) | 10 cc dual syringe with the static mixer | **805998-3EA** |
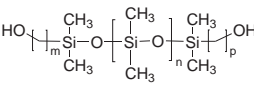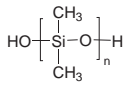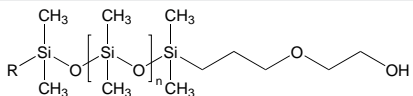
### Hydride (H) Terminated PDMS

| Name | Structure | Molecular Weight | Viscosity (cSt) | Cat. No. |
|---|---|---|---|---|
| Poly(dimethylsiloxane), hydride terminated | | average $M_n$ ~580 | - | **423785-50ML** **423785-250ML** |
| | | average $M_n$ ~17,500 | ~500 | **482064-100ML** |
| | | average $M_n$ ~24,000 | ~1,000 | **482145-100ML** |
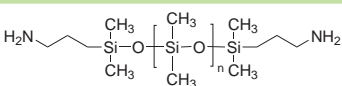
### Methyl ($CH_3$) Terminated PDMS

| Name | Structure | Viscosity (cSt) | Cat. No. |
|---|---|---|---|
| Hexamethyldisiloxane | | 0.65 | **469300-50ML** **469300-250ML** |
| Poly(dimethylsiloxane) | | 1.0 | **469319-50ML** |
| Poly(methylhydrosiloxane) | | ~3 | **482382-20ML** |
| | | 12-45 | **176206-50G** **176206-250G** |

### Hydroxy (OH) Terminated PDMS
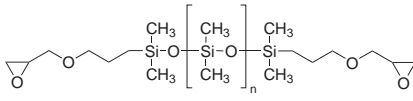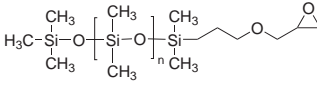
| Name | Structure | Viscosity | Cat. No. |
|---|---|---|---|
| Poly(dimethylsiloxane), bis(hydroxyalkyl) terminated | | 100 cP | **481246-25ML** **481246-100ML** |
| Poly(dimethylsiloxane), hydroxy terminated | | ~25 cSt | **481939-100ML** **481939-500ML** |
| | | ~65 cSt | **481955-100ML** **481955-500ML** |
| | | ~750 cSt | **481963-100ML** **481963-500ML** |
| | | 2550-3570 cSt | **432989-100ML** **432989-500ML** |
| | | 3,500 cSt | **482161-250ML** |
| | | 18,000-22,000 cSt | **432997-100ML** **432997-500ML** |
| | | ~50,000 cSt | **482005-100ML** |
| Poly(dimethylsiloxane), monohydroxy terminated | | ~79 cSt | **480355-50ML** |

### Amine ($NH_2$) Terminated PDMS
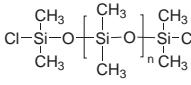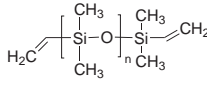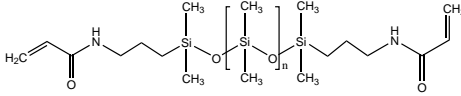
| Name | Structure | Molecular Weight | Viscosity (cSt) | Cat. No. |
|---|---|---|---|---|
| Poly(dimethylsiloxane), bis(3-aminopropyl) terminated | | average $M_n$ ~2,500 | 50 | **481688-10ML** **481688-50ML** |
| | | average $M_n$ ~27,000 | 2,000 | **481696-50ML** |

## Epoxy Terminated PDMS

| Name | Structure | Molecular Weight | Viscosity (cSt) | Cat. No. |
|---|---|---|---|---|
| Poly(dimethylsiloxane), diglycidyl ether terminated | | average $M_n$ ~800 | 15 | **480282-50ML** **480282-250ML** |
| Poly(dimethylsiloxane), monoglycidyl ether terminated | | average $M_n$ ~5,000 | ~65 | **480290-25ML** |

## Other End Group Functionalized PDMS

| Name | Structure | Molecular Weight | Viscosity (cSt) | Cat. No. |
|---|---|---|---|---|
| Poly(dimethylsiloxane), chlorine terminated | | average $M_n$ ~3,000 | ~3 | **481653-50ML** |
| Poly(dimethylsiloxane), vinyl terminated | | average $M_w$ ~25,000 | 850-1,150 | **433012-100ML** **433012-500ML** |
| Polydimethylsiloxane-diacrylamide | | average $M_n$ 1,200 | - | **798266-1G** |
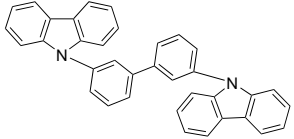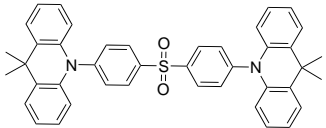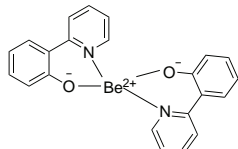
## OLED and PLED Materials

For a complete list of available materials, visit **SigmaAldrich.com/oel**.

### Light-Emitting Polymers

| Name | Molecular Weight | Cat. No. |
|---|---|---|
| Super yellow light-emitting PPV copolymer | average $M_n$ >400,000 average $M_w$ >1,300,000 | **900438-1G** |
| Orange light-emitting PPV copolymer | average $M_n$ 340,000 average $M_w$ 1,750,000 | **900440-1G** |
| Green light-emitting spiro-copolymer | average $M_n$ >100,000 average $M_w$ >400,000 | **900441-250MG** |
| Red light-emitting spiro-copolymer | average $M_n$ 50,000 average $M_w$ 180,000 | **900444-250MG** |
| | average $M_n$ 105,000 average $M_w$ 470,000 | **900447-250MG** |
| | average $M_n$ 120,000 average $M_w$ 720,000 | **900446-250MG** |
| F8BT | average $M_n$ >20,000 average $M_w$ >20,000 | **900979-250MG** |
| | average $M_w$ 10,000-20,000 | **900978-250MG** |
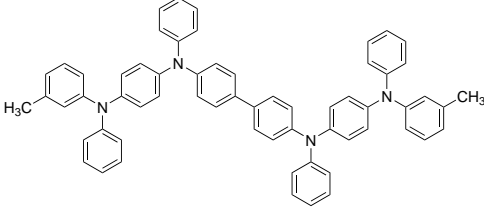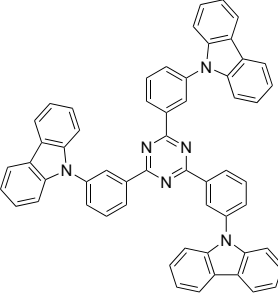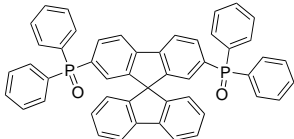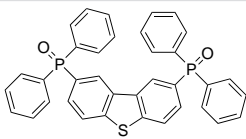
### Light Emitters and Dopants

| Name | Structure | Purity | Cat. No. |
|---|---|---|---|
| m-CBP | | >99%, HPLC (sublimed) | **900938-250MG** **900938-1G** |
| DMAC-DPS | | >99%, HPLC (Sublimed) | **900940-250MG** **900940-1G** |
| Bepp$_2$ | | >99%, HPLC (sublimed) | **900959-100MG** **900959-500MG** |

| Name | Structure | Purity | Cat. No. |
|------|-----------|--------|----------|
| mDCBPy | | ≤98% | **901039-500G** |
| Ir(MDQ)₂(acac) | | >99%, HPLC (sublimed) | **901074-100MG**<br>**901074-500MG** |
| Hex-Ir(piq)₃ | | >99% | **901104-100MG** |
| FIr6 | | >99% | **901106-100MG** |
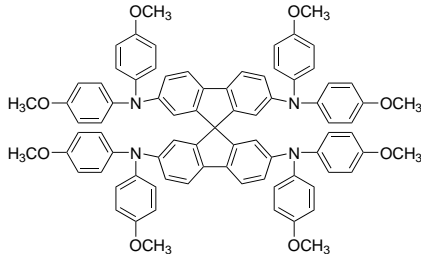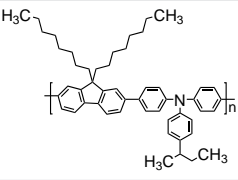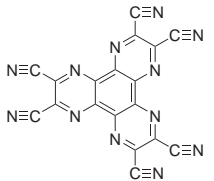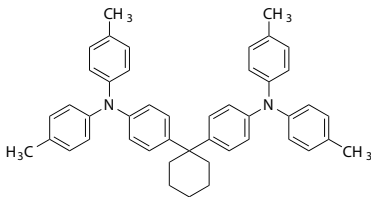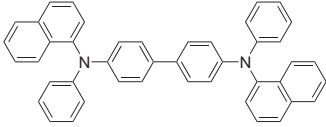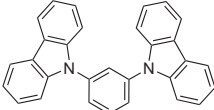
## Host Materials

| Name | Structure | Purity | Cat. No. |
|------|-----------|--------|----------|
| 2,6-Bis(9H-carbazol-9-yl)pyridine | | ≥98% | **900922-500MG** |
| 9-Phenyl-9'-(triphenylsilyl)-3,3'-bicarbazole | | ≤97% | **900963-250MG** |
| DPTPCz | | ≤97% | **900964-500MG** |
| CzSi | | ≤97% | **900965-500MG** |

| Name | Structure | Purity | Cat. No. |
|---|---|---|---|
| N,N'-Diphenyl-N,N'-bis-[4-(phenyl-m-tolylamino)phenyl]biphenyl-4,4'-diamine | | ≥98% | **900968-250MG** |
| TCPZ | | ≥98% | **900969-500MG** |
| SPPO13 | | >99%, HPLC | **900977-100MG**<br>**900977-500MG** |
| PPT | | >99% (sublimed) | **901102-250MG**<br>**901102-1G** |
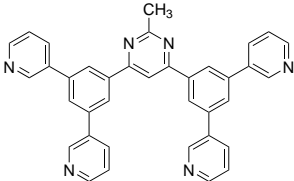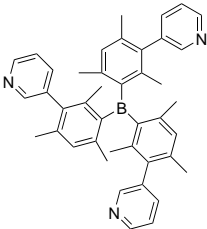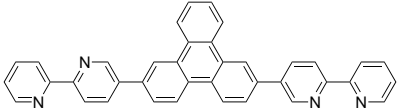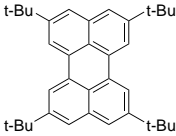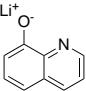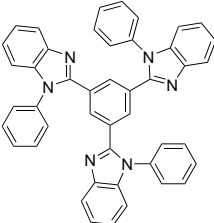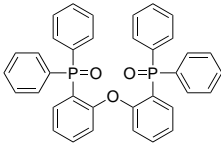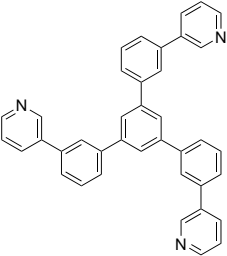
## Hole Transport Material

| Name | Structure | Purity/Molecular Weight | Cat. No. |
|---|---|---|---|
| Spiro-MeOTAD | | 99%, HPLC | **792071-1G**<br>**792071-5G** |
| TFB | | average $M_w$ >30,000  by GPC | **901101-250MG**<br>**901101-1G** |
| 2,2',7,7'-Tetrakis(N,N-diphenylamino)-9,9-spirobifluorene | | 99%, HPLC | **765007-1G** |
| Dipyrazino[2,3-f:2',3'-h]quinoxaline-2,3,6,7,10,11-hexacarbonitrile | | 97%, HPLC | **764957-1G** |

| Name | Structure | Purity/Molecular Weight | Cat. No. |
|------|-----------|-------------------------|----------|
| 4,4'-Cyclohexylidenebis[N,N-bis(4-methylphenyl)benzenamine] | | 97% | **757284-1G**<br>**757284-5G** |
| N,N'-Di(1-naphthyl)-N,N'-diphenyl-(1,1'-biphenyl)-4,4'-diamine | | 96% | **734594-5G** |
| 1,3-Bis(N-carbazolyl)benzene | | 97% | **701874-5G** |

## Electron Transport and Hole Blocking Materials

| Name | Structure | Purity/Molecular Weight | Cat. No. |
|------|-----------|-------------------------|----------|
| B$_3$PYMPM | | >99%, HPLC (sublimed) | **900958-100MG**<br>**900958-500MG** |
| 3TPYMB | | >99%, HPLC (sublimed) | **900953-100MG**<br>**900953-500MG** |
| BPy-TP2 | | >99%, HPLC (sublimed) | **900939-100MG**<br>**900939-500MG** |
| TBPE | | >99%, HPLC (sublimed) | **900937-250MG** |
| Liq | | >99.5%, HPLC (sublimed) | **900928-1G** |
| TPBi | | ≥99.5%, HPLC | **806781-500MG** |
| DPEPO | | 98% | **805459-5G** |

| Name | Structure | Purity/Molecular Weight | Cat. No. |
|---|---|---|---|
| TmPyPB | | 99%, HPLC | **790907-1G**<br>**790907-5G** |

## Carbon Nanotubes

For a complete list of available materials, visit **SigmaAldrich.com/cnt**.

### Single-Walled Carbon Nanotubes

| Production Method | Dimensions | Purity | Cat. No. |
|---|---|---|---|
| Catalytic Carbon Vapor Deposition (CCVD) Method | average diameter 2 nm | >70% | **755710-250MG**<br>**755710-1G** |
| CoMoCAT™ Catalytic Chemical Vapor Deposition (CVD) Method | average diameter 0.84 nm | ≥95% (≥99% as carbon nanotubes) | **775533-250MG**<br>**775533-1G** |
| | average diameter 0.83 nm | ≥90% (≥99% as carbon nanotubes) | **704121-250MG**<br>**704121-1G** |
| | average diameter 0.78 nm | ≥95% (≥99% as carbon nanotubes) | **773735-250MG**<br>**773735-1G** |
| | average diameter 0.78 nm | ≥90% (≥99% as carbon nanotubes) | **704148-250MG**<br>**704148-1G** |
| | diameter 1.3 nm | ≥90% (≥80% as carbon nanotubes) | **724777-250MG**<br>**724777-1G** |
| | average diameter 0.82 nm<br>diameter 0.7 - 1.3 nm | ≥89% (≥99% as carbon nanotubes) | **704113-250MG**<br>**704113-1G** |
| Electric Arc Discharge Method | D × L 2-10 nm × 1-5 µm (bundle dimensions)<br>1.3-1.5 nm (individual SWNT diameter) | 40-60 wt. % | **698695-1G**<br>**698695-5G** |
| | diameter 1.2 - 1.7 nm<br>L 0.3-5 µm | 2% (Metallic)<br>98% (Semiconducting) | **750522-1MG** |
| | diameter 1.2 - 1.7 nm<br>L 0.3-5 µm | 30% (Metallic)<br>70% (Semiconducting) | **750514-25MG** |
| | diameter 1.2 - 1.7 nm<br>L 0.3-5 µm | 30% (Metallic)<br>70% (Semiconducting) | **750492-100MG** |
| | diameter 1.2 - 1.7 nm<br>L 0.3-5 µm | 2% (Semiconducting)<br>98% (Metallic) | **750530-1MG** |

### Double-Walled Carbon Nanotubes

| Production Method | Dimensions | Purity, | Cat. No. |
|---|---|---|---|
| Catalytic Carbon Vapor Deposition (CCVD) Method | avg. diam. × L<br>3.5 nm × >3 µm (TEM) | Metal Oxide ≤10% TGA | **755141-1G** |
| | avg. diam. × L<br>3.5 nm × 1-10 µm (TEM) | Metal Oxide <10% TGA | **755168-1G** |
| Chemical Vapor Deposition (CVD) Method | O.D. × I.D. × L<br>5 nm × 1.3-2.0 nm × 50 µm | 50-80% carbon basis | **637351-250MG**<br>**637351-1G** |

### Multi-Walled Carbon Nanotubes

| Production Method | Description | Purity | Cat. No. |
|---|---|---|---|
| CoMoCAT™ synthesis process | D × L 2.5-3 nm × 2-6 µm<br>Deposition temp: 550 ± 50 °C<br>G/D ratio: ≥10 (Raman)<br>Median number of walles: 2 to 3 (TEM) | ≥94%(carbon as CNT by TGA)<br>moisture content ≤5 wt. % TGA | **900788-1G**<br>**900788-250MG** |
| Chemical Vapor Deposition (CVD) Method | O.D. × L 10-40 nm × 0.5-1.5 mm<br>diam. × L 10-40 nm × 0.5-1.5 mm<br>flake of bundled CNTs | >95% carbon basis | **901002-1G** |
| | aspect ratio >100 (by FE-SEM)<br>D/G ratio: 0.1 (by Raman spectroscopy) | >99.5% carbon basis(by X-ray fluorescence) | **901019-25G** |
| | O.D. × L 6-13 nm × 2.5-20 µm<br>12 nm (average diameter, HRTEM)<br>10 µm (average length, TEM) | >98% carbon basis | **698849-1G** |
| | D × L 110-170 nm × 5-9 µm | >90% carbon basis | **659258-2G**<br>**659258-10G** |

| Production Method | Description | Purity | Cat. No. |
|---|---|---|---|
| Catalytic Carbon Vapor Deposition (CCVD) Method | avg. diam. × L 9.5 nm × <1 μm (TEM) thin and short | Metal Oxide <5% TGA | **755117-1G** |
| | avg. diam. × L 9.5 nm × 1.5 μm (TEM) thin | Metal Oxide <5% TGA | **755133-5G** |
| Electric Arc Discharge Method | O.D. × L 7-12 nm × 0.5-10 μm powdered cylinder cores | 20-30% MWCNT basis | **406074-500MG** **406074-1G** **406074-5G** |
| | O.D. × L 7-15 nm × 0.5-10 μm as-produced cathode deposit | >7.5% MWCNT basis | **412988-100MG** **412988-2G** **412988-10G** |
| Plasma-Enhanced Chemical Vapor Deposition (PECVD) Method | diam. × L 100-150 nm × 30 μm (SEM) vertically aligned on silicon wafer substrate | >95 atom % carbon basis(x-ray) | **687804-1EA** |

# Organic Photovoltaic Applications for IoT, Architecture, and Wearables

Graham Morse,[1] Richard Harding,[1*] Nicolas Blouin,[2] Hannah Buerckstrummer[2]
Not pictured: Agnieszka Pron,[1] Stephan Wieder,[2] David Mueller,[2] and Stephane Berny[3]

[1]Merck Chemicals Ltd, Chilworth Technical Centre, University Parkway, Southampton. SO16 7QD, U.K.
[2]Merck KGaA, Frankfurter Str. 250, 64293 Darmstadt I Germany
[3]Merck Selbstmedikation GmbH, Frankfurter Str. 250, 64293 Darmstadt, Germany
*Email: richard.harding@merckgroup.com

## Introduction

The development of high performance carbon-based semiconductors has enabled organic photovoltaics (OPVs) to become an important source of alternative energy over the past few years. The newly developed active materials used in OPV are non-toxic and enable cost effective and eco-friendly roll-to-roll manufacturing with orders of magnitude lower energy consumption compared to the manufacturing process for classic photovoltaics. As a result, OPV systems have significantly faster payback times versus other solar technologies.[1-3] OPV modules are thin and flexible laminates that can easily be added to a variety of substrates and building materials, including standard lamination onto glass. Furthermore, OPV systems do not exhibit a drop in performance caused by typical outdoor conditions such as diffuse light and high temperatures. The versatility to adapt and tune active materials enables the creation of modular designs that meet specific requirements including a choice of colors, shapes, and degrees of transparency. This allows OPV to meet many more functional and aesthetic demands required by product designers and architects.[4] OPV technology was recently used to fabricate a >250 $m^2$ flexible power system reaching an average performance of ~5% power conversion efficiency (PCE) in a semi-transparent configuration, as illustrated in **Figure 1**.[4]

The Internet of Things (IoT) is rapidly developing and connecting everyday physical objects to the internet in order to identify and communicate with other devices. The IoT has attracted tremendous interest because of its potential positive impact on quality of life and the enormous pool of new business opportunities that it is expected to enable. Early benefits of IoT can be found in engineering, logistics, transportation, and operation processes.[5] A recent analysis by McKinsey summarized the potential business impact of IoT and concluded that the market for these technologies is expected to increase as much as 11 trillion USD by 2025.[6] One key technical prerequisite for the growth of IoT is the ability for developers to create
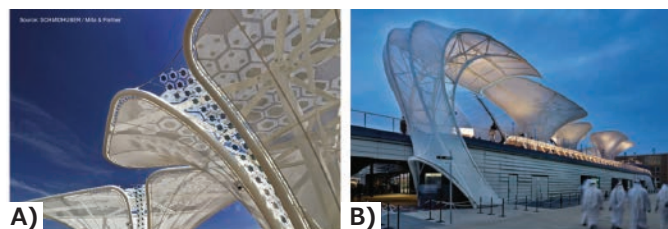


**Figure 1.** OPV Solar Trees at EXPO 2015 in Milan. **A**) Series of OPV solar modules fabricated by solution-deposition techniques (blue hexagons on the picture) are connected to form a network of >250 m2 charging batteries during daylight. **B**) OPV-powered lights coming from the trunk of the Solar Trees create aesthetic shades during the night.

innovative hardware infrastructure using cost-effective, low-energy, and maintenance-free power sources for use in offices, human wellness, and retail. Photovoltaic (PV) technologies are seen as particularly interesting energy-harvesting systems for IoT because of its potential for low-power output and portability in miniaturized and grid-independent applications.

For these reasons, interest in OPV as an energy source for architectural elements, IoT, and wearable devices is increasing. In this review, we outline some recent progress in OPV materials and device design, and detail examples of where OPV technology can act as an energy source, potentially enabling larger deployment of low-power, low-maintenance, and environmentally friendly hardware solutions.

## OPV Solar Cell Design

Solution processed organic photovoltaic systems were first tested by Heeger and Sariciftci.[7] The bulk heterojunction (BHJ) concept was later developed[8] to minimize the mean path length that excitons must diffuse while maximizing light absorption within the device. The accessibility of modern synthetic

techniques and tools for molecular engineering of aromatic systems has allowed for a great material diversity in BHJ solar cells. BHJ solar cell efficiencies in the lab have increased from ~3%[8] to better than 12%[9] over the past 20 years. As a result, OPV is now generating significant commercial interest and promises to have an impact on a number of new applications, both large and small.

## BHJ Concept

BHJ solar cells are fabricated by the coating or printing of subsequent layers to form a multilayered stack in which each layer plays a specific role in charge generation, separation, or extraction. Since each layer is printed from inks of soluble components, it is essential that each layer be designed to avoid dissolution of the underlying layers — a property known as orthogonality. Two main device configurations exist for BHJ solar cells, commonly referred to as standard and inverted architectures (**Figure 2**). These architectures are constructed starting with a transparent conductor, usually indium tin oxide (ITO) or ITO-metal-ITO (IMI) patterned on top of a transparent substrate such as glass or plastic (PET or PEN). Next, a layer designed to selectively allow the passage of holes or electrons is applied to the transparent surface of the conductor. These layers, known as interlayers, blocking layers, or transport layers come from a wide variety of material classes, ranging from organic molecules and polymers, to metals and metal oxides. The most popular blocking layers are PEDOT:PSS (**See page 124 for a list of available catalogue numbers**), or molybdenum oxide (**Cat. No. 203815**) as electron blocking layers (EBL) that form the anode and zinc oxide, PFN, and PEIE as hole blocking layers (HBL) that form the cathode. These materials are designed to be soluble in polar solvents to facilitate their orthogonality with the subsequent BHJ, which is most soluble in non-polar aromatic solvents.

The bulk heterojunction is formed from two components. Both the donor and acceptor are mutually dissolved in a common solvent system. Upon drying of the ink, donor- and acceptor-rich phases form in the resulting film, giving rise to the bulk heterojunction, an interdigitated donor and acceptor network. The donor component is designed to transport holes, and the acceptor component is designed to transport electrons. Excitons separate into free charges at the interface making a high surface area between these two components desirable. These materials can be either organic small molecules or polymers, but the most popular systems contain polymeric donor materials and soluble small molecule acceptors. The polymers employed in high performance BHJ solar cells are not limited in design and diversity, the best of which cover a range of band gaps which dictate the ability of the material to absorb light and give rise to a wide variety of colors. Finally, the complementary blocking layer is applied on top of the BHJ, followed by a top electrode which can either be opaque or transparent. In a majority of cases the top electrode is fabricated from silver, aluminium, or PEDOT:PSS, either alone or in combination.
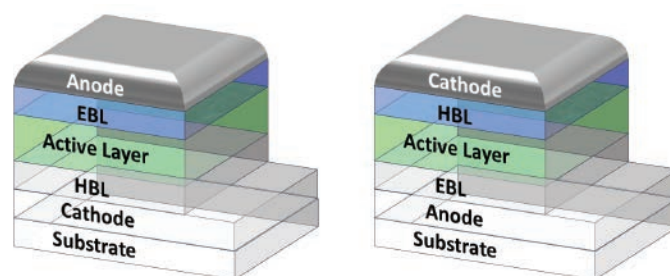


**Figure 2.** Schematic view of common standard and inverted BHJ solar cell architectures.

## OPV Materials Development

### Materials Design

Tremendous progress has been made in the field of OPV materials over the last 20 years.[8,9] These improvements are the result of both a better understanding of the working principles of OPV devices and the development of new, more suitable organic materials. Since BHJ is a mixture of donor (designed to transfer holes) and acceptor (designed to transfer electrons) materials (**Figure 3**), interdigitation allows an efficient separation of excitons into free charges. Commonly, BHJ consist of polymeric, oligomeric, or defined small molecules, pi-conjugated donors and fullerene acceptors.[10]
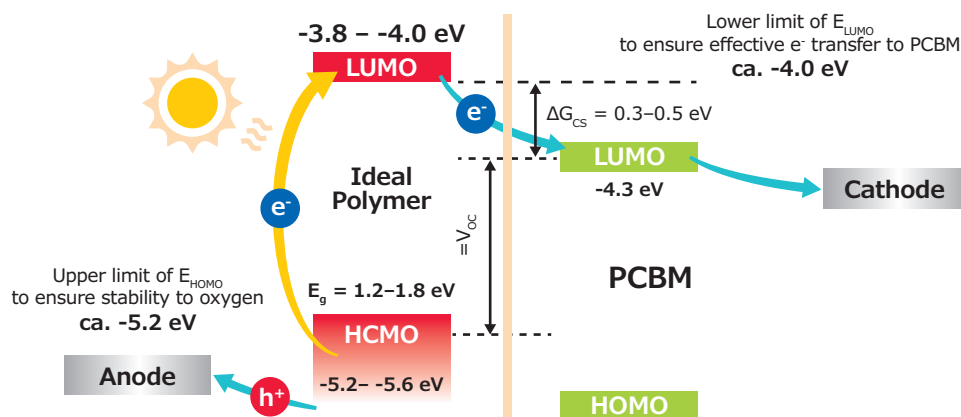


**Figure 3.** Working principle of OPV using the concept of the difference between the highest occupied molecular orbital (HOMO) and lowest unoccupied molecular orbital (LUMO) creating the band-gap for a donor polymer (same applies to oligomers and small molecules).

When blended with a fullerene derivative, the optimal donor polymers have (1) highest occupied molecular orbital (HOMO) energy levels below -5.1 eV to ensure air stability and effective charge separation at the polymer:fullerene/small molecule interface, which results in high open circuit voltage (Voc), (2) lowest unoccupied molecular orbital (LUMO) energy levels in the range of -3.6 to -4.0 eV to create enough driving force to promote an exciton dissociation, and (3) relatively low energy band gap (1.2 to 1.9 eV) with a broad absorption spectrum to absorb as much sun light as possible to generate high closed or short circuit current (Jsc). Additionally, materials should be readily soluble in common non-chlorinated organic solvents to allow easy processability.

There are two main approaches used to achieve low-band gap conjugated materials. The first involves incorporation of units that promote formation of quinoid structures in the excited state. The second approach is based on incorporating alternating electron donating and electron accepting moieties in the material backbone (**Figure 4**). Usually, the HOMO energy level of the polymer is derived from the electron rich moiety, whereas the LUMO energy level is derived from the electron poor unit. This approach allows very precise tuning of both energy levels as well as solubility profile of the resulting materials.
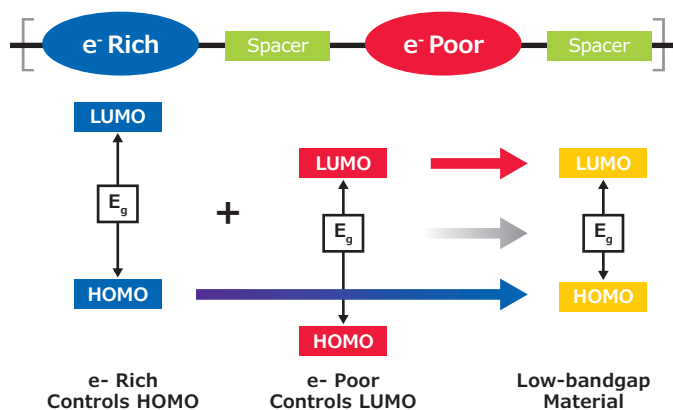


**Figure 4.** Design principles of low-band gap OPV materials

OPV materials can be synthesised by various transition metal catalyzed cross-coupling reactions. The three main approaches shown in **Figure 5** are used for the synthesis of these semiconducting polymers.
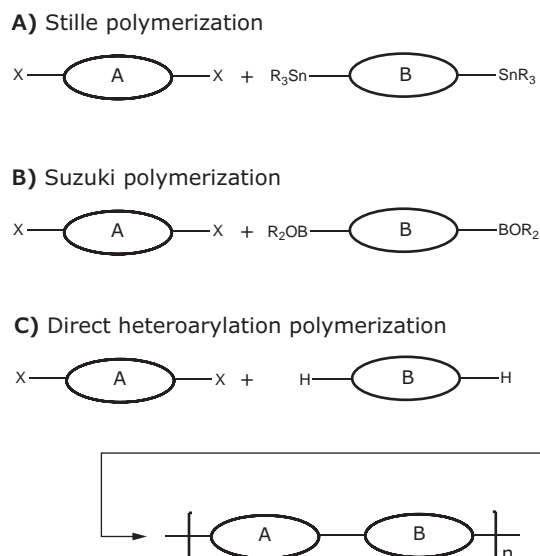


**Figure 5.** Polymerization reactions used for OPV polymers

Stille polymerization is the most versatile method for the synthesis of conjugated polymers. It is a very robust technique that works for most of the known highly electron rich monomers, such as thiophene and related derivatives. However, a key drawback is the extra cost required for the safe handling of the precursors and waste stream.[11] An alternative method involves Suzuki polymerization.[12] However, the suitability of the monomers, or functional groups towards Suzuki conditions is limited, particularly for electron rich monomers like thiophene and related derivatives used in OPV. More recently, direct heteroarylation polymerization has been used.[13] It does not require preparation and purification of organometalic species, thus making synthesis shorter and more cost effective. Yet only a handful of monomers were found suitable for direct heteroarylation polymerization and much more in depth research is needed to fully understand the potential and limitations of this synthetic method. Many modern small molecules and oligomers have been prepared using similar coupling methodologies.

## Future Prospects

There has been significant focus by the research community on the design of new donor materials. Some of the most important donor polymers are shown in **Figure 6**. This figure perfectly illustrates the changes in material design.[14-19] Alongside polymer development, small molecule donor materials have also been developed. Bazan et al. achieved efficiencies above 7% from their small molecule donor materials.[20]
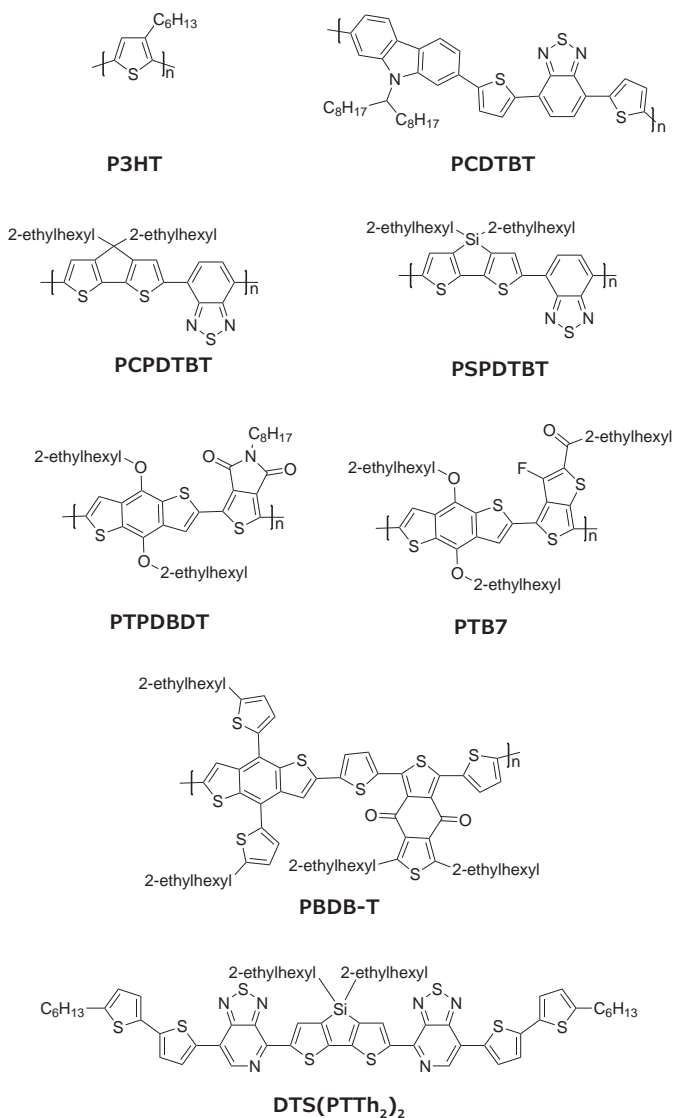


**Figure 6.** Examples of donor materials for OPV

Until recently, acceptor materials have been almost exclusively based on fullerenes (**Figure 7**). Much research in this field has focused on fine-tuning the HOMO-LUMO energy levels in order to gain higher Voc in BHJ OPV and increase the solubility of the materials.[21,22]

However, since 2014, the performance of OPV cells using non-fullerene acceptors (NFA) has increased dramatically, with efficiencies increasing from 5% in 2014[23] to 12% in the end of 2016.[24] Moreover, the solubility and energy levels of NFA materials have the potential to be tuned to give more flexibility than conventional fullerene acceptors. NFA are also strong light absorbers, meaning that they contribute to the overall EQE of the device. All of these points add to the versatility of these materials.[25] The field of NFA is still very immature, but it is believed that use of NFA will enable researchers to reach power conversion efficiencies up to 20%.
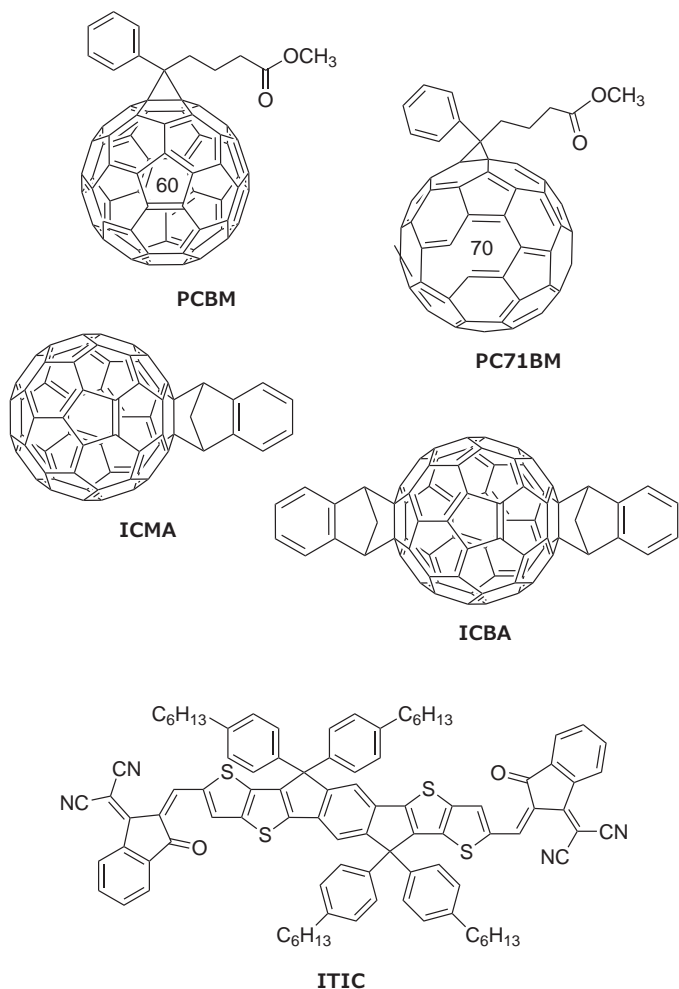


**Figure 7.** Examples of OPV acceptor materials

## OPV Applications

OPV technology can be tuned to create a unique choice of colors and shades (**Figure 8A**). It also inherently enables greater design freedom, because OPV systems are lightweight and manufactured from solution-deposition techniques in which printing or laser structuration can easily be incorporated (**Figure 8B** and **8C**). These properties are key enablers for low-power IoTs, since many applications require: (1) customized design and form factors, (2) higher performance and lifetime, (3) low-maintenance energy-harvesting systems and interoperability between devices and locations. Here, we will focus on three applications of OPV including urban architecture, indoor IoT, and wearables.
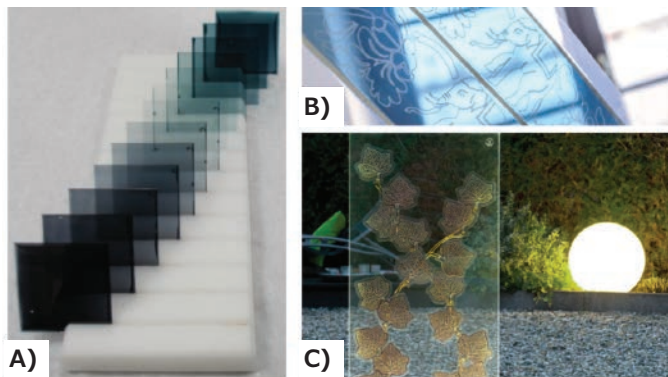


**Figure 8.** Inherent freedom of design of OPV. **A**) PV-F series (OPV active inks developed by EMD Performance Materials) offer a choice of colors and shades while maintaining compatibility with large schale roll-to-roll processing equipment for manufacturing OPV modules. **B**) Customized design elements on OPV printed system by OPVIUS. **C**) Elektree: OPV-powered lamp by OPVIUS GmbH, made by connecting a series of leaf-shaped OPV modules.

### OPV Urban Facades

One aim of integrating OPV technology into facade elements is to reduce both the energy consumption and $CO_2$ emission of a building. This global trend is demonstrated in the United States by schemes like the Leadership in Energy and Environmental Design (LEED) program. The European Union has set a target for new buildings to be nearly zero energy by 2021. This requires significant effort in energy managements systems and smart building envelopes. The recently updated EU legislative package, includes a proposal for a "Smartness Indicator" (SI) to characterize a building's ability to interact with its occupants as well as to manage the overall energy consumption of connected energy assets by itself.[26]

Modern smart buildings are expected to contain a manifold of interacting systems, extending beyond the heating, ventilation, and air conditioning systems commonly found in current buildings. Systems for managing lighting, security and safety, energy demand, and personalization features will become much more common. The use of energy-harvesting surfaces (glass or membranes) in urban environments is expected to be a key enabler for the larger deployment of the various IoT applications that currently rely on power from the grid or from batteries with limited lifetime and require frequent maintenance. Examples of these wireless solutions are sensors and small motorized systems for ventilation[27] and shading.[6]

Compared to classic PV technology, OPV can better serve both the functional and aesthetic demands of designers and architects while also enabling the use of building-integrated photovoltaics. OPV modules have been integrated into various glass facades and into structural membrane architectures. One example is the African Union Peace and Security Building in Addis Ababa where OPV is used to power lights throughout the building, significantly reducing its thermal load (**Figure 9A**). A more recent example of OPV integration into building elements was developed by a collaboration between OPVIUS GmbH and BGT Bischoff Glas Technik AG, supervised by Timo Carl Architecture, Kassel in 2016 (**Figure 9D**). Here, OPV modules were laminated into glass-facades of an exterior elevator shaft attached to an existing building in Marburg, Germany. The electricity produced is used to ventilate the shaft and prevent heat accumulation. A major breakthrough was achieved by demonstrating these glass-facades comply with German safety standards and building regulations. Another more recent example of OPV installation is the OPV facade created by SUNEW, Brazil.
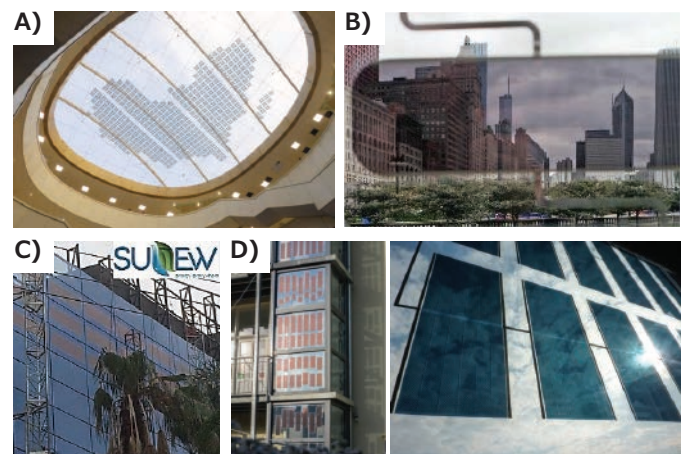


**Figure 9.** A) OPV sail in shape of African continent using EMD Performance Materials PV-F series and OPVIUS technology at the African Union Peace and Security Building in Addis Ababa. **B**) Gray-colored OPV modules made with PV-F series from Lisicon, by OPVIUS GmbH, demonstrating efficiencies of 50 W/m$^2$. Picture taken at the Adaptative Architectures and Smart Materials Conference in Chicago, USA. **C**) OPV elements installed by SUNEW in a building in Sao Paolo, Brazil. **D**) OPV glass-façade used to ventilate an exterior elevator in Marburg, Germany.

In the urban context new applications are expected to emerge with wider distribution of smart parking meters, centralized traffic-control systems, active displays, or even the management of autonomous vehicles. One interesting approach takes advantage of the lightweight property of OPV modules through integration into bus shelters or other infrastructure to support the development of "connected cities" (**Figure 10A**). Such applications not only increase consumer safety by providing power for lighting during the night, but also enabling other devices such as sensors for probing air quality or temperature, connected hardware for real-time traffic monitoring, or electronic charging stations.
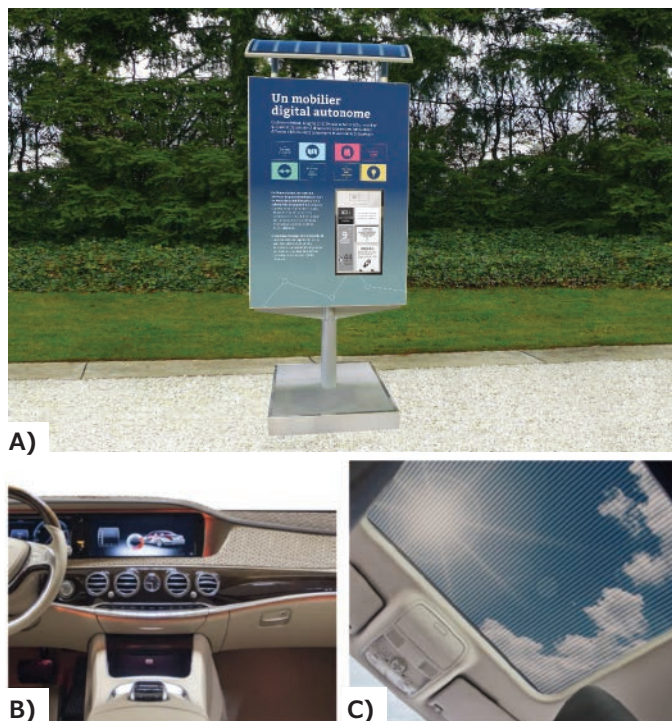




**Figure 10. A**) Conceptual design for off-grid kiosks and display invented by JCDecaux in collaboration with Armor that combine mobile technology, e-paper display and ASCA© photovoltaic films. **B**) Artist view of the interior of a concept car equipped with multiple IoT applications that use OPV to harvest energy. **C**) Roof of a car equipped with OPV that could be used to block the sun, improve energy efficiency, and supply energy for IoT devices. Concept A is equipped with ARMOR ASCA OPV film and concepts **B** and **C**) with OPVIUS GmbH Technology.

## OPV for Indoor IoT

While a reference standard light spectrum has been developed for outdoor applications (AM1.5), such a standard is missing for indoor light tests due to the large variations in light sources such as fluorescent light, LED, incandescent lamps, sun coming through windows (**Figure 12A**).[28] The most commonly used light sources in home or office environments are fluorescent lamps or white LEDs, and as a result they are the most commonly used lighting for technical studies. Their illuminance is usually

in the region of 200 lux (living room environment) to 1000 lux (office environment), corresponding to a light intensity of around 100 to 500 times lower than 1 Sun condition. Under indoor conditions, low power indoor devices such as wireless sensor network nodes consume power in the region of few mW.[29] Well-established photovoltaic technologies such as silicon solar cells have already been shown to provide adequate power under such low-light levels. The use of photovoltaic technologies in this type of environment is promising for the fabrication of low-maintenance devices, in addition to being more environmentally-friendly than commercial batteries. As a result, a number of indoor products have emerged within the last few years using photovoltaic technologies, including several that integrate OPV (**Figure 11**).[29,30]

In the case of indoor IoT applications, OPV addresses several inherent weaknesses in PV systems by enhancing design flexibility and aesthetic appeal, reducing weight, and most importantly, increasing efficiency under low-light conditions, leading to a smaller system footprint. In a recent study, Cutting et al. reported that the efficiency of OPV devices can be increased up to 350% under LED light intensity relative to outdoor conditions (**Figure 12B**). This performance is significantly higher than that of competing Si-technologies or Perovskite-type cells under the same irradiance. OPV devices used in this study can reach efficiencies of more than 20% PCE, higher than their inorganic counterparts.[31]
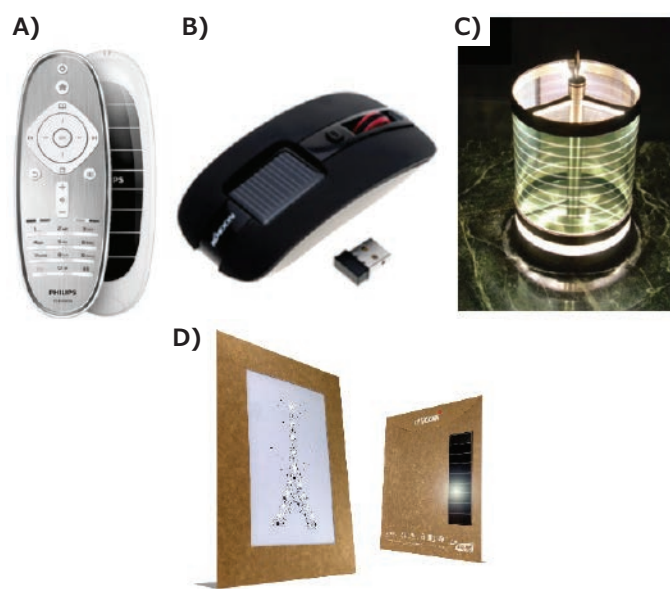


**Figure 11. A**) Philips remote control **B**) Solar computer mouse by Wholesale **C**) Indoor lighting made with a curved OPV module by .STOOL. **D**) 'Citigami' , the latest creation from LITOGAMI in collaboration with Armor, is a collection of poetic, entertaining, educational, and decorative cards neatly incorporating an ultra-light and ultra-flexible ASCA© photovoltaic film as its sole source of energy.
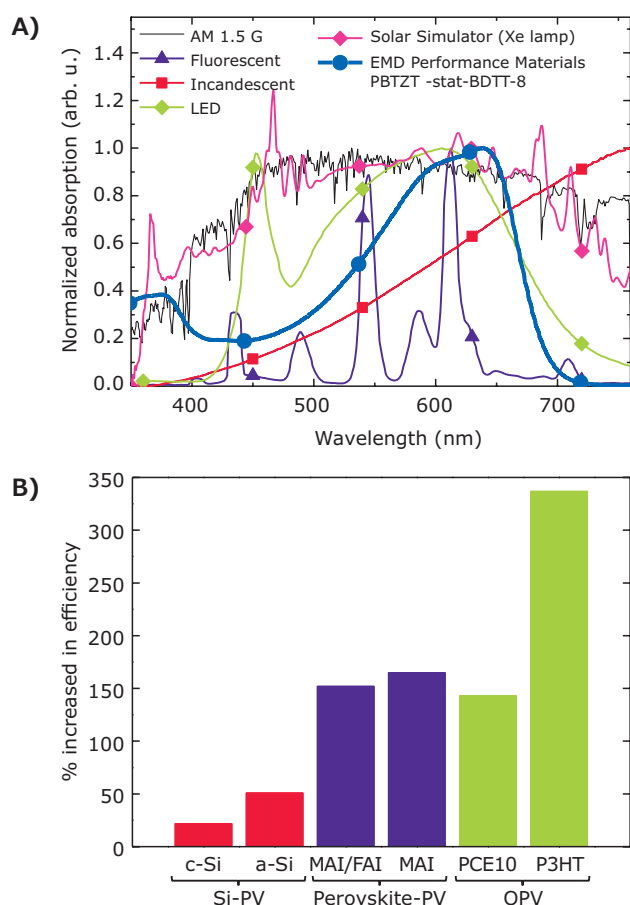
**Figure 12. A)** Normalized power spectra of different light sources: 1 Sun AM1.5G (line), incandescent light bulb 2800 K (red squares), solar simulator with xenon lamp (brown diamond), CFL 6500 K (purple triangles), LED (green diamond), and the normalized absorption spectrum of an organic solar cell using a BHJ made of PBTZ-stat-BDTT-8 donor material and PV-A600 acceptor material (blue circle). **B)** The percent increase in power conversion of various photovoltaic systems under white LED relative to outdoor conditions. Data for graph **B** compiled from reference 31 with permission.

Another study by Lee et al., shows some specific OPV systems using a combination of the donor polymer PCDTBT (**Cat. 753998**) and the PCBM[70] acceptor materials (**Cat. No. 684465**) can reach more than 16% PCE under 300 lux fluorescent lamp.[32] Interestingly, this BHJ system is not the highest performing under outdoor conditions. The researchers explain that the best performing system benefits here from an optimal energy gap that matches the irradiance spectrum of the light source.[32] This system delivers a power output of 13.9 µW/cm$^2$ under 300 lux, which is higher than gallium arsenide and polycrystalline silicon cells reported by Teran et al. at 12.5 µW/cm$^2$ and 2.5 µW/cm$^2$, respectively, under the same conditions.[33] In another study, De Rossi et al. extracted powers of 12.5 µW/

cm$^2$ and 9.1 µW/cm$^2$ under 300 lux fluorescent lamp irradiance from DSSC and a-Si, respectively.[34] Finally, Lee et al. showed the power output obtained with OPV modules of 100 cm$^2$ can reach almost 1 mW, opening the door to multiple use in photo-rechargeable systems under low light conditions, also recently demonstrated by Lechene et al.[28] with super capacitors.

Overall, these studies highlight that OPV systems already achieve high efficiency in low-light environments. Contrary to other PV technologies, the optical absorption profile of OPV systems can be finely tuned by various means, such as by varying the molecular design of the donor and/or acceptor components, changing their ratio in the BHJ, or by defining a process window that favors certain defined morphologies. These intrinsic properties increase the freedom of design and ease of integration, making OPV technology ideal for future indoor IoT applications.

The integration of flexible and highly-sensitive energy harvesting systems such as OPV is expected to benefit a number of aspects in future smart homes, including connected thermostats or wireless sensors. The potential applications become even broader when considering the retail industry where IoT applications have the potential to revolutionize inventory management processes and sales analytics. In this sector, IoT is seen as a game changer throughout the value chain, including improved store layouts and live-tracking of inventory, to name just a few applications.

## OPV for Wearables IoT

Ever since the semiconducting properties of organic materials were first demonstrated in devices, significant attention has been devoted to integrating these technologies into wearable systems. In the case of OPV, Krebs et al. first described a series of fundamental strategies for the integration of OPVs into garments and textiles.[35] This work was followed by a variety of approaches by other researchers that tried to solve the challenges of integrating OPV with wearable surfaces. To do so, researchers have focused on developing new materials, new deposition techniques, and innovative stacks for OPV devices.

To this end, O'Connor et al. developed a system on a polyimide substrate that can be worn on the skin. The authors sacrificed the charge transport properties of the OPV materials by integrating non-optimized donor polymer material into the BHJ and additives to the other layers in order to increase plasticization behavior.[36] By doing this, they demonstrated a vast improvement in mechanical robustness (stretchability) of the OPV devices when submitted to cycles of deformation bending

compared to standard devices that use P3HT as the donor material (**Figure 13A**). Another approach reported by Lee et al., used organic solar cells stitched onto a textile functionalized by conductive fibers.[37] A PCE of about 2% was obtained for the system. Digging deeper into stack prototyping, Gaudiana et al. published a breakthrough approach with the design of OPV wires that could be used as textile fibers.[38] The optoelectronic viability of the stack is ensured by a customized co-axial design of the wire, which enables the device to exceed the performance of standard planar geometries (**Figure 13B**). For the most part, these studies demonstrated the potential of OPV integration with fabrics, but did not advance beyond single lab prototypes. In an effort to accelerate the application and scalability of the technology, the Advanced Structures and Composite Center at the University of Maine has produced 40,000 feet of OPV wires

with an efficiency of 7%, and created 40 ft$^2$ of woven fabric from OPV wires.[39]

In parallel to these efforts, several electronic wearables and portable products have been developed for commercial use over the past few years, paving the way for IoT technologies. Markets where these technologies are expected to have an impact include healthcare (diagnostics, wellness monitoring), clothing, augmented reality, fitness, and security. **Figures 14B,C,** and **D**, show commercial examples in which OPV has been used in outdoor gear such as tents, backpacks and waterproof jackets. **Figure 14A** shows a smart bag, which connects via Bluetooth to a smart-phone, powered by OPV. The bag highlights incoming messages and calls and sounds an alarm if the phone is left behind.
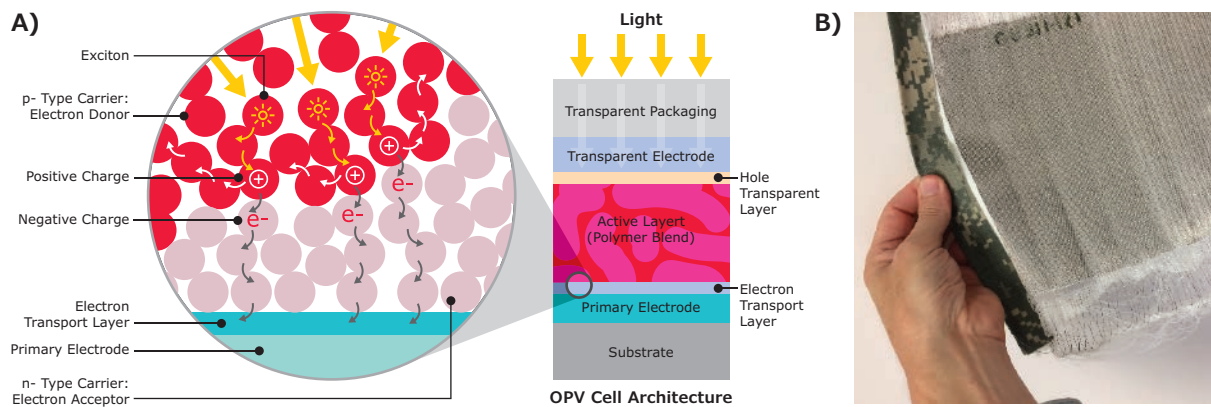


**Figure 13.** A) Schematic view describing a working OPV cell. B) Photograph showing woven cloth comprised of OPV wires. Image and photo courtesy of the Advanced Structures and Composite Center at the University of Maine



**Figure 14.** A) Tailor-made smart bag by Kolon Industries, integrating organic solar module energy-harvester (wrapped by red rectangle) and NFC technology. B) Star Tent by Kolon Industries, integrating LED lighting with OPV as the energy-source. C) Smart jacket integrating an OPV module, LED, and Bluetooth by Kolon Industries. D) Backpack by Kolon Industries, integrating OPV as power source for cooling fans. E) Solar bag designed and manufactured by Armor using ASCA© photovoltaic films as source of energy.

## Conclusion

OPV technology demonstrates a number of enabling properties for products that require energy harvesting systems. Compared to existing power source alternatives, OPV offers added value in terms of performance, environmental friendliness, design customization, and form factor.

To date, the first applications of OPV technology have started to emerge with installation in smart buildings, urban facades and membranes, indoor/low-light products, as well as wearables and portables. We anticipate the continuous improvement of OPV systems will further enable its implementation in a wider scope of markets including retail, worksites, homes, and transportation.

## References

(1) Krebs, F. C.; Espinosa, N.; Hosel, M.; Sondergaard, R. R. *Adv. Mater.* **2014**, *26*, 29.

(2) Espinosa, N; Hosel, M.; Angmo, D.; Krebs, F. C. *Energy Environ. Sci.* **2012**, *5*, 5117.

(3) Emmott, C. J. M.; Ekins-Daukes, N. J.; Nelson, J. *Energy Environ. Sci.* **2014**, *7*, 1810.

(4) Berny, S.; Blouin, N.; Distler, A.; Egelhaaf, H. J.; Krompiec, M.; Lohr, A.; Lozman, O. R.; Morse, G. E.; Nanson, L.; Pron, A., *Adv. Sci.* **2015**, *3*(5), 1500342.

(5) Macaulay, J.; Buckalew, L.; Chung, G. *Internet of Things in Logistics* DHL Trend Reasearch & Cisco Consulting Services, Troisdorf, Germany, **2015**.

(6) Manyika, J.; Chui, M.; Bisson, P.; Woetzel, J.; Dobbs, R.; Bughin, J.; Aharon, D. *The Internet of Things : Mapping the Value Beyond the Hype.* McKinsey Global Institute **2015**. http://www.mckinsey.com/business-functions/digital-mckinsey/our-insights/the-internet-of-things-the-value-of-digitizing-the-physical-world (accessed September 20, 2017)

(7) Sariciftci, N.S.; Smilowitz, L.; Heeger, A.J.; Wudl, F. *Science* **1992**, *258*(5087), 1474-1476, DOI:10.1126/science.258.5087.1474.

(8) Yu, G.; Gao, J.; Hummelen, J.C.; Wudl, F.; Heeger, A. *Science* **1995**, *270*, 1789-1791, DOI:10.1126/science.270.5243.1789.

(9) Li, S.; Ye, L.; Zhao, W.; Zhang, S.; Mukherjee, S.; Ade, H.; Hou, J. *Adv. Mater.* **2016**, *28*(42), 9423-9429, DOI:10.1002/adma.201602776.

(10) Günes, S.; Neugebauer, H.; Sariciftci, N. S. Chem. Rev. **2007**, *107*(4), 1324-1338, DOI:10.1021/cr050149z.

(11) Stille, J. K. *Angew. Chem. Int. Ed. Engl.* **1986**, *25*, 508–524, DOI:10.1002/anie.198605081.

(12) Miyaura, N.; Suzuki, A. *Chem. Rev.* **1995**, *95*(7), 2457–2483, DOI:10.1021/cr00039a007.

(13) Berrouard, P.; Najari, A.; Pron, A.; Gendron, D.; Morin, P.-O.; Pouliot, J.-R.; Veilleux, J.; Leclerc, M. *Angew. Chem. Int. Ed.* **2012**, *51*, 2068-2071, DOI:10.1002/anie.201106411.

(14) Yu, G.; Nishino, H.; Heeger, A. J.; Chen, T.-A.; Rieke R. D. *Synth. Met.* **1995**, *72*(3), 249-52, DOI:10.1016/0379-6779(95)03282-7.

(15) Wakim, S.; Beaupré, S.; Blouin, N.; Aich, B.-R.; Rodman, S.; Gaudiana, R.; Tao, Y.; Leclerc, M. *J. Mater. Chem.* **2009**, *19*, 5351-5358, DOI:10.1039/B901302D.

(16) Muehlbacher, D.; Schraber, M.; Morana, M.; Zhu, Z.; Waller, D.; Gaudiana, R.; Brabec, C. *Adv. Mater.* **2006**, *18*, 2884–2889, DOI:10.1002/adma.200600160.

(17) Hou, J.; Chen, H.-Y.; Zhang, S.; Li, G.; Yang, Y. *J. Am. Chem. Soc.* **2008**, *130*(48), 16144–16145., DOI:10.1021/ja806687u.

(17) Zou, Y.; Najari, A.; Berrourard, P.; Beaupre, S.; Aich, B. R.; Tao, Y.; Leclerc, M. *J. Am. Chem. Soc.* **2010**, *132*(15), 5330-5331, DOI:10.1021/ja101888b.

(19) Zhao, W.; Qian, D.; Zhang, S.; Li, S.; Inganäs, O.; Gao, F.; Hou, J. *Adv. Mater.* **2016**, *28*, 4734–4739. DOI:10.1002/adma.201600281.

(20) Sun, Y.; Welch, G. C.; Leong, W. L.; Takacs, C.; Bazan, G. C.; Heeger, A. J *Nat. Mater.* **2012**, *11*, 44-4 (2012), DOI:10.1038/nmat3160.

(21) Wudl, F. *Acc. Chem. Res.* **1992**, *25*(3), 157-161, DOI:10.1021/ar00015a009.

(22) Nardes, A. M.; Ferguson, A. J.; Whitaker, J. B.; Larson, B. W.; Larsen, R. E.; Maturová, K.; Graf, P. A.; Boltalina, O. V.; *Adv. Funct. Mater.* **2012**, *22*, 4115–4127, DOI:10.1002/adfm.201200336.

(23) Lin, Y.; Wang, J.; Zhang, Z.-G.; Bai, H.; Li, Y.; Zhu, D.; Zhan, X. *Adv. Mater.* **2015**, *27*, 1170–1174, DOI:10.1002/adma.201404317.

(24) Ye, L.; Zhao, W.; Li, S.; Mukherjee, S.; Carpenter, J. H.; Awartani, O.; Jiao, X.; Hou, J.; Ade, H. *Adv. Energy Mater.* **2016**, *7*(7), 1602000, DOI:10.1002/aenm.201602000.

(25) Lin, Y.; Zhao, F.; Wu, Y.; Chen, K.; Xia, Y.; Li, G.; Prasad, S. K. K.; Zhu, J.; Huo, L.; Bin, H.; Zhang, Z.-G., Guo, X.; Zhang, M.; Sun, Y.; Gao, F.; Wei, Z.; Ma, W.; Wang, C.; Hodgkiss, J.; Bo, Z.; Inganäs, O.; Li, Y.; Zhan, X. *Adv. Mater.* **2017**, *29*, 1604155.

(26) http://www.buildup.eu/en/practices/publications/european-commission-proposal-revised-energy-performance-buildings-directive-0 (accessed September 20, 2017)

(27) Merck KGaA, Darmstadt, Germany. (2017). *Innovation Award for Organic Photovoltaics at the BAU* [Press release]. Retrieved from https://www.emdgroup.com/en/news/opv-innovation-award-19-01-2017.html

(28) Lechêne, B. P.; Cowell, M.; Pierre, A.; Evans, J. W.; Wright, P. K.; Arias, A. C. *Nano Energy* **2016**, *26*, 631-640.

(29) Minnaert, B.; Veelaert, P. *Adv. Sci. Tech.* **2010**, *74*, 170-175.

(30) Apostolou, G.; Reinders, A.; Verwaal, M. *Energy Science & Engineering* **2016**, *4*(1), 69-85.

(31) Cutting, C. L.; Bag, M.; Venkataraman, D. *J. Mater. Chem. C* **2016**, *4*(43), 10367-10370.

(32) Lee, S.; Lee, Y.; Park, J.; Choi, D. *Nano Energy* **2014**, *9*, 88-93.

(33) Teran, A. S.; Wong, J.; Lim, W.; Kim, G.; Lee, Y.; Blaauw, D.; Phillips, J. D., *IEEE Trans. Electron Devices* **2015**, *62*, 2170.

(34) De Rossi, F.; Pontecorvo, T.; Brown, T. M., *Appl. Energy* **2015**, *156*, 413.

(35) Krebs, F.C.; Biancardo, M.; Winther-Jensen, B.; Spanggard, H.; Alstrup, J. *Sol. Energy Mater. Sol. Cells* **2006**, *90*, 1058–1067.

(36) O'Connor, T. F.; Zaretski, A. V.; Savagatrup, S.; Printz, A. D.; Wilkes, C. D.; Diaz, M. I.; Sawyer, E. J.; Lipomi, D. J. *Sol. Energy Mater. Sol. Cells* **2016**, *144*, 438-444.

(37) Lee, S.; Lee, Y.; Park, J.; Choi, D. *Nano Energy* **2014**, *9*, 88-93.

(38) Lee, M. R.; Eckert, R. D.; Forberich, K.; Dennler, G.; Brabec, C.- J.; Gaudiana, R. A. *Science* **2009**, *324*, 232-235.

(39) Private communication, David Erb, Advanced Structures and Copsite Center, University of Maine.
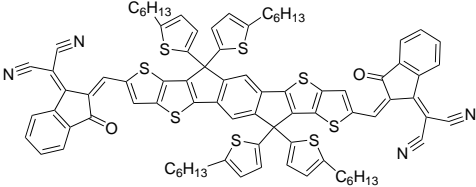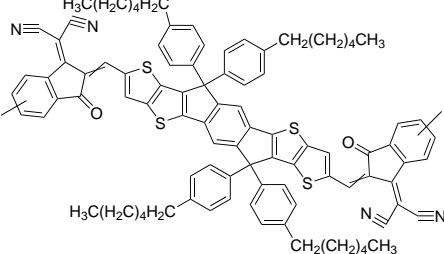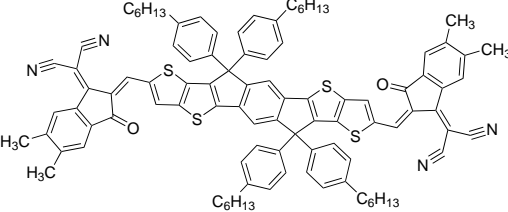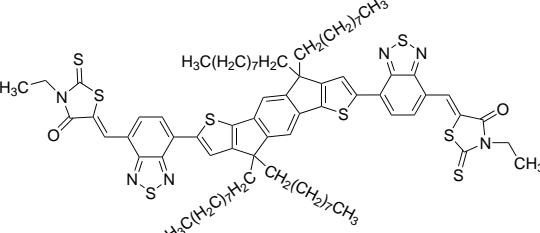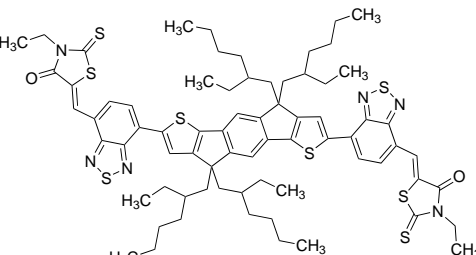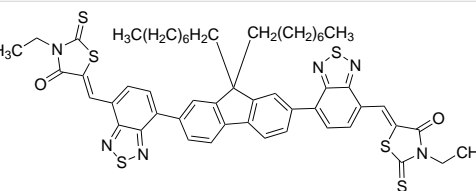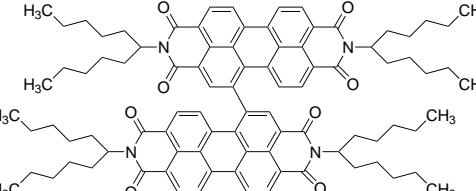
## OPV Donor Materials

For a complete list of available materials, visit **SigmaAldrich.com/oel**.

| Name | Structure | Molecular Weight | Cat. No. |
|------|-----------|------------------|----------|
| PffBT4T-2OD | | $M_w$ 100,000-150,000  by GPC | **900720-100MG** |
| J61 | | $M_w$ 50,000-100,000  by GPC (PS standard) | **901045-100MG** |
| J51 | | $M_w$ 40,000-80,000  by GPC (PS standard) | **901058-100MG** |
| PBDB-T | | $M_w$ >50,000  by GPC (PC standard) | **901099-100MG** |
| PDBT-T1 | | $M_w$ >35,000  by GPC (PS standard) | **901097-100MG** |

| Name | Structure | Molecular Weight | Cat. No. |
|---|---|---|---|
| PBDTTT-C-T |  | average $M_w$ 80,000-120,000 | **901067-100MG** |
| PDPP2T-TT-OD |  | average $M_w$ 40,000-60,000  by GPC | **791989-100MG** |
| PBDTBO-TPDO |  | average $M_n$ 10,000-50,000 | **777080-100MG** |
| PBDT-TPD |  | average $M_n$ 10,000-50,000 | **776300-100MG** |
| PBDT(EH)-TPD(Oct) |  | - | **773514-100MG** |
| PTB7 |  | average $M_w$ 80,000-200,000 | **772410-100MG** |

| Name | Structure | Molecular Weight | Cat. No. |
|---|---|---|---|
| PBDTTT-CF | | average $M_w$ 53,000-83,000 by GPC | **772402-100MG** |
| PSiF-DBT | | average $M_n$ 10,000-80,000 | **754021-100MG** |
| PFO-DBT | | average $M_w$ 10,000-50,000 | **754013-100MG** |
| PCPDTBT | | average $M_w$ 7,000-20,000 | **754005-100MG** |
| PCDTBT | | average $M_w$ 100,000-140,000 | **753998-100MG** |
| PDTSTPD | | average $M_n$ 7,000-35,000 by GPC | **745928-100MG** |
| PBTTPD | | average $M_n$ 3,500-20,000 g/mol | **745901-100MG** |
| TQ1 | | average $M_n$ 12,000-45,000 g/mol | **745898-100MG** |

## Non-Fullerene Acceptors

For a complete list of available materials, visit **SigmaAldrich.com/oel**.

| Name | Structure | Purity/Molecular Weight | Cat. No. |
|---|---|---|---|
| ITIC | | 99% | **900799-100MG**<br>**900799-50MG** |

| Name | Structure | Purity/Molecular Weight | Cat. No. |
|---|---|---|---|
| ITIC-Th |  | 99% | **900800-50MG** <br> **900800-100MG** |
| IT-M |  | 99% | **900947-50MG** <br> **900947-100MG** |
| IT-DM |  | 99% | **900803-50MG** <br> **900803-100MG** |
| O-IDTBR |  | 99% | **900810-100MG** <br> **900810-50MG** |
| EH-IDTBR |  | 99% | **900853-50MG** <br> **900853-100MG** |
| FBR |  | 99% | **900854-50MG** <br> **900854-100MG** |
| 2,2',9,9'-Tetrakis(1-pentylhexyl)-[5,5'-bianthra[2,1,9-def:6,5,10-d'e'f']diisoquinoline]-1,1',3,3',8,8',10,10'(2H,2'H,9H,9'H)-octone |  | 99%, NMR | **900774-100MG** |

| Name | Structure | Purity/Molecular Weight | Cat. No. |
|---|---|---|---|
| SF-PDI | | 99% | **900782-100MG** |
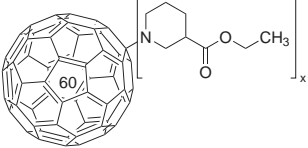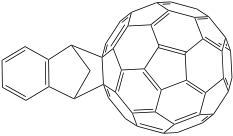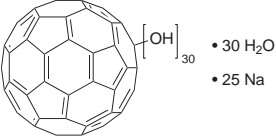
## Fullerenes

For a complete list of available materials, visit **SigmaAldrich.com/oel**.
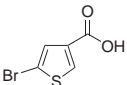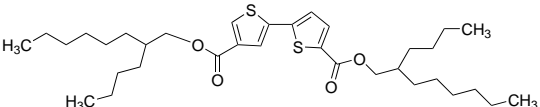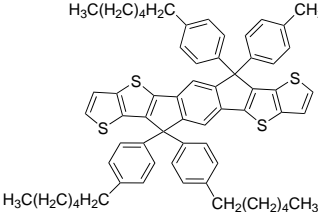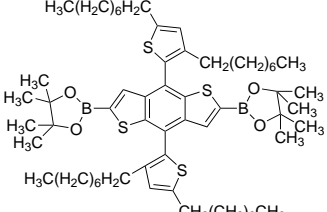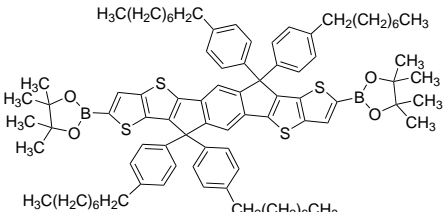
| Structure | Name | Purity | Cat. No. |
|---|---|---|---|
| | [6,6]-Phenyl $C_{71}$ butyric acid methyl ester, mixture of isomers | 99% | **684465-100MG** **684465-500MG** |
| | [6,6]-Phenyl $C_{61}$ butyric acid methyl ester | >99.9% | **684457-100MG** |
| | | >99.5% | **684449-100MG** **684449-500MG** |
| | | >99% | **684430-1G** |
| | [6,6]-Pentadeuterophenyl $C_{61}$ butyric acid methyl ester | 99.5% | **684503-100MG** |
| | [6.6] Diphenyl $C_{62}$ bis(butyric acid methyl ester) (mixture of isomers) | 99.5% | **704326-100MG** |
| | [6,6]-Phenyl-$C_{61}$ butyric acid butyl ester | >97% | **685321-100MG** **685321-1G** |
| | [6,6]-Phenyl-$C_{61}$ butyric acid octyl ester | ≥99% | **684481-100MG** |
| | [6,6]-Thienyl $C_{61}$ butyric acid methyl ester | ≥99 | **688215-100MG** |
| | N-Methylfulleropyrrolidine | 99% | **668184-100MG** |

| Structure | Name | Purity | Cat. No. |
|---|---|---|---|
| | Small gap fullerene-ethyl nipecotate | ≥95%, fullerenes 50% | **707473-250MG** |
| | ICMA | 97% | **753947-250MG** |
| | ICBA | 99% | **753955-250MG** |
| | Polyhydroxy small gap fullerenes, hydrated | Polyhydroxy SGFs(TGA) ~85% | **707481-100MG** |
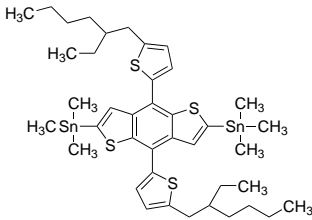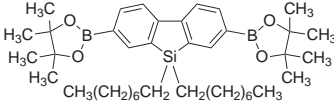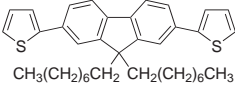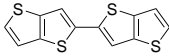
## Thiophene Monomers and Building Blocks

For a complete list of available materials, visit **SigmaAldrich.com/oel**.

| Name | Structure | Purity | Cat. No. |
|---|---|---|---|
| 5-Bromothiophene-3-carboxylic acid | | >98% | **900764-250MG** |
| [2,2'-Bithiophene]-4,4'-dicarboxylic acid, 4,4'-bis(2-butyloctyl) ester | | >98% | **900745-250MG** |
| 6,6,12,12-Tetrakis(4-hexylphenyl)-6,12-dihydro-dithieno[2,3-d:2',3'-d']-S-indaceno[1,2-b:5,6-b']dithiophene | | >98% | **900754-250MG** |
| 4,8-Bis(3,5-dioctyl-2-thienyl)-2,6-bis(4,4,5,5-tetramethyl-1,3,2-dioxaborolan-2-yl)benzo[1,2-b:4,5-b']dithiophene | | >98% | **900765-500MG** |
| 6,12-Dihydro-6,6,12,12-tetrakis(4-octylphenyl)-2,8-bis(4,4,5,5-tetramethyl-1,3,2-dioxaborolan-2-yl) dithieno[2,3-d:2',3'-d']-s-indaceno[1,2-b:5,6-b']dithiophene | | >98% | **900766-500MG** |

| Name | Structure | Purity | Cat. No. |
|---|---|---|---|
| 2,8-Dibromo-6,12-dihydro-6,6,12,12-tetrakis(4-octylphenyl)-dithieno[2,3-d:2',3'-d']-s-indaceno[1,2-b:5,6-b']dithiophene | | >98% | **900767-500MG** |
| 2,2'-Thieno[3,2-b]thiophene-2,5-diylbis-3-thiophenecarboxylic acid | | >98% | **900778-500MG** |
| 5-Octylthieno[3,4-c]pyrrole-4,6-dione | | ≥99% | **773859-1G** |
| 1,3-Dibromo-5-octyl-4H-thieno[3,4-c]pyrrole-4,6(5H)-dione | | ≥99.5%, HPLC | **766585-1G** |
| 1,3-Dibromo-5-(2-ethylhexyl)-4H-thieno[3,4-c]pyrrole- 4,6(5H)-dione | | 97% | **759910-1G** |
| 4,7-Dibromobenzo[c]-1,2,5-thiadiazole | | 99.5%, GC | **778109-1G** |
| 4,7-Dibromo-5-fluoro-2,1,3-benzothiadiazole | | ≥99%, HPLC | **746630-1G** |
| 4,7-Bis(2-bromo-5-thienyl)-2,1,3-benzothiadiazole | | ≥99.0%, HPLC | **732435-1G** |
| 1,3-Dibromo-5-heptyl-4H-thieno[3,4-c]pyrrole-4,6(5H)-dione | | 99%, HPLC | **747114-1G** |
| Benzo[1,2-b:4,5-b']dithiophene-4,8-dione | | 97% | **760137-1G** |
| 2,6-Bis(trimethyltin)-4,8-bis(2-ethylhexyloxy)benzo[1,2-b:4,5-b']dithiophene | | 99%, HPLC | **765023-1G**<br>**765023-5G** |

| Name | Structure | Purity | Cat. No. |
|---|---|---|---|
| 2,6-Bis(trimethylstannyl)-4,8-bis(2-ethylhexyloxy)benzo[1,2-b:4,5-b']dithiophene | | 99.5%, HPLC | **766550-500MG** |
| 9,9-Dioctyl-9H-9-silafluorene-2,7-bis(boronic acid pinacol ester) | | 97% | **760102-500MG** |
| 2,2'-(9,9-Dioctyl-9H-fluorene-2,7-diyl)bisthiophene | | 97% | **763985-1G** |
| 2,2'-Bithieno[3,2-b]thiophene | | 96% | **752908-1G** |

## Indium Tin Oxide (ITO) Coated Substrates

For a complete list of available materials, visit **SigmaAldrich.com/ito**.

| Name | L × W × Thickness (mm) | Surface Resistivity (Ω/sq) | Cat. No. |
|---|---|---|---|
| Indium tin oxide coated PET | 1 ft × 1 ft × 5 mil | 60 | **639303-1EA**<br>**639303-5EA** |
| | | 100 | **639281-1EA**<br>**639281-5EA** |
| | | 200 | **749745-1EA**<br>**749745-5EA** |
| | | 250 | **749761-1EA**<br>**749761-5EA** |
| | | 300 | **749796-1EA**<br>**749796-5EA** |
| | 1 ft × 1 ft × 7 mil | 60 | **749729-1EA**<br>**749729-5EA** |
| | | 100 | **749737-1EA**<br>**749737-5EA** |
| | | 200 | **749753-1EA**<br>**749753-5EA** |
| | | 250 | **749788-1EA**<br>**749788-5EA** |
| | | 300 | **749818-1EA**<br>**749818-5EA** |
| Indium tin oxide coated glass slide, square | 25 × 25 × 1.1 | 8-12 | **703192-10PAK** |
| | | 30-60 | **703184-10PAK** |
| | | 70-100 | **703176-10PAK** |
| Indium tin oxide coated glass slide, rectangular | 75 × 25 × 1.1 | 8-12 | **578274-10PAK**<br>**578274-25PAK** |
| | | 15-25 | **636916-10PAK**<br>**636916-25PAK** |
| | | 30-60 | **636908-10PAK**<br>**636908-25PAK** |
| | | 70-100 | **576352-10PAK**<br>**576352-25PAK** |

# Ferroelectrics Solved with Solvene® Electro Active Polymers

Print on the leading edge with our Solvene® electro-active polymers (EAPs). This family of ferroelectric polymers and ferrorelaxor polymers combines excellent electromechanical properties with easy processing.

Solvene® P(VDF-TrFE) copolymers are inherently piezo-, pyro- and ferroelectric, enabling applications in printed memory, sensors, actuators, loudspeakers, acoustic transducers, and energy-harvesting devices.

Solvene® materials can be processed by applying various techniques, from classic extrusion to printing on flexible plastic films and paper.
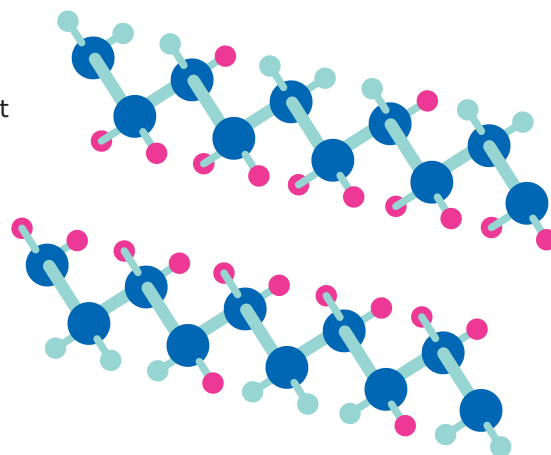
● Carbon
● Fluorine
● Hydrogen

## Key Features

- Transparent
- Piezoelectric Coefficient (D33) ≥ -22pC/N
- Curie Temperature: up to 131 °C

| Name | Description | Cat. No. |
|------|-------------|----------|
| Solvene® 200/P200 | VDF 80 % mol., TrFE 20% mol., average molecular weight 200 Curie Peak: 131 +/-3 °C | **900895** |
| Solvene® 200/P400 | VDF 80 % mol., TrFE 20% mol., average molecular weight 400 Curie Peak: 131 +/-3 °C | **900903** |
| Solvene® 250/P300 | VDF 75 % mol., TrFE 25 % mol., average molecular weight 300 Curie Peak: 114 +/-3 °C | **900905** |
| Solvene® 250/P400 | VDF 75 % mol., TrFE 25 % mol., average molecular weight 400 Curie Peak: 114 +/-3 °C | **900904** |
| Solvene® 300/P300 | VDF 70 % mol., TrFE 30 % mol., average molecular weight 300 Curie Peak: 103 +/-3 °C | **900906** |

To find out more about ferroelectric polymers, visit **SigmaAldrich.com/FEP**.

# Flexible and Printed Organic Thermoelectrics: Opportunities and Challenges
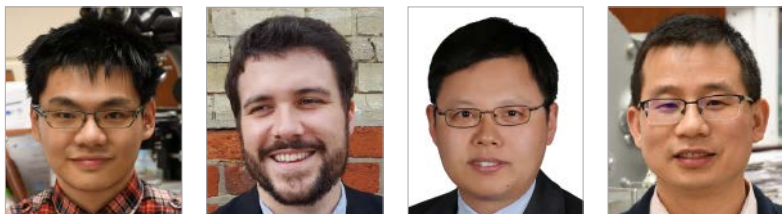
Xuyi Luo,[1] Bob C. Schroeder,[2*] Chong-an Di,[3*] Jianguo Mei[1*]

[1]Department of Chemistry, Purdue University, 560 Oval Dr. West Lafayette, IN, 47907, USA.
[2]The Organic Thermoelectric Laboratory, Materials Research Institute and School of Biological & Chemical Sciences, Queen Mary University of London, Mile End Road, London E1 4NS, United Kingdom.
[3]Beijing National Laboratory for Molecular Sciences, CAS Key Laboratory of Organic Solids, Institute of Chemistry, Chinese Academy of Sciences, Beijing 100190, China.
*Email: b.c.schroeder@qmul.ac.uk, dicha@iccas.ac.cn and, jgmei@purdue.edu

## Introduction

Technologies that promote sustainable energy are experiencing unprecedented interest due to the growing population and the need to meet higher living standards. According to the United States Department of Energy, up to 50 percent of the energy from all fuels burned in the U.S. ends up in the environment as waste heat.[1] If the waste heat from commercial and industrial operations could be collected and converted to electricity, it would fulfill up to 20 percent of the total U.S. electricity demand. Thermoelectrics directly converts thermal energy into electrical energy and is among the most promising renewable energy technologies.

Thermoelectric materials, when placed into a thermal gradient, generate an electrical potential due to the Seebeck effect (**Figure 1**). The reverse process is known as the Peltier effect. The temperature gradient causes the diffusion of charge carriers with the resulting electrical potential directly proportional to the temperature differences across the material,

$$S = \frac{\Delta V}{\Delta T}$$

where $S$ is the Seebeck coefficient. The thermoelectric figure of merit, ZT is defined as,

$$ZT = \frac{S^2 \sigma T}{k}$$

with $\sigma$ the electrical conductivity and $k$ the thermal conductivity. The Seebeck coefficient $s$, characteristic of the average entropy per charge transport, should be large in order to create a high voltage induced by a temperature gradient. The Seebeck

coefficient, however, is not the only parameter to be optimized in order to maximize ZT. The electrical conductivity $\sigma$, must be large to minimize the joule heating dissipation during the charge transport. Besides the two parameters mentioned, a good thermoelectric material should also feature low thermal conductivity $k$, to prevent heat flow through the material. The difficulty of designing high performance thermoelectric materials arises from the fact that both electrical and thermal conductivity are related via the carrier concentration; optimizing one parameter will negatively affect the other.[2] This interdependence has hindered the development of thermoelectric materials for many years. While progress has been made in inorganic nanostructured materials, the increasing complexity in material design complicates the introduction of thermoelectric generators as an alternative energy technology to the mass market due to high manufacturing costs and sophisticated fabrication processes.
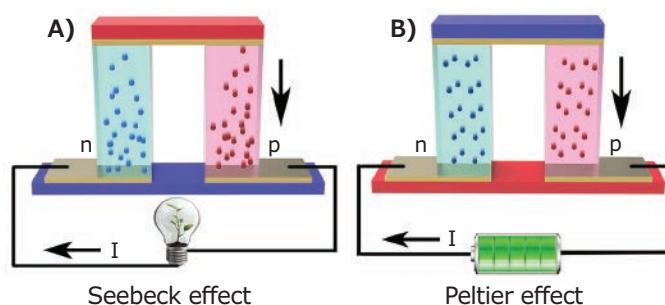


**Figure 1.** Operation principle of a **A**) thermoelectric generator and **B**) Peltier device. A thermoelectric device generally consisted of p- and n-type thermoelectric materials connected in series through conducting plates.

Organic thermoelectric materials have attracted increased attention as an alternative approach to conventional thermoelectronics and are experiencing rapid development. These materials are particularly attractive for low-quality waste heat harvesting. Several conventional organic semiconductors exhibit good thermoelectric performances. High ZT values (over 0.1) have been achieved for both p-type and n-type organic thermoelectric materials.[3,4] Both inorganic and organic thermoelectrics are described as "electronic crystals and phonon glasses". In contrast to inorganic thermoelectrics, the study of organic thermoelectrics aims to achieve "electronic crystals", because organic semiconductors have intrinsically low thermal conductivities. Increasing $S^2$, namely Power Factor (PF), is the main route to enhance the performance of organic thermoelectrics. The expression of electrical conductivity ($\sigma$), where e is electrical charge for each carrier, µ is the mobility, and n is the concentration of carriers is shown here:

$$\sigma = e\mu n$$

However, the Seebeck coefficient $S$ typically decreases with increasing carrier concentration. This trade-off between $S$ and $\sigma$ requires optimization of power factors, which is currently achieved by precisely tuning the doping level.

## Progress in Organic Thermoelectric Materials

Organic semiconductors have been largely neglected as thermoelectric materials, despite their inherent low thermal conductivities ($\approx$ 0.3 W m$^{-1}$ K$^{-1}$) and high electrical conductivities

(> 1,000 S cm$^{-2}$).[5-6] Two of the challenges encountered in developing organic thermoelectrics are the carrier concentrations and the device architecture. First, it is essential to control the charge carrier density of organic semiconductors by doping in order to attain high electrical conductivities and Seebeck coefficients. Second, the most common thermoelectric generator architecture relies on two semiconductor legs, one p-type and one n-type, connected thermally in parallel, but electrically in series. A list of representative p- and n-type semiconducting polymers and dopants are listed in **Figure 2**.

The most successful p-type material developed to date is undoubtedly, poly(3,4-ethylenedioxy thiophene) polystyrene sulfonate (PEDOT:PSS), a polyelectrolyte consisting of positively charged PEDOT and negatively charged PSS. PEDOT:PSS is commercially available as a dispersion in water, which facilitates processing and greatly contributes to its popularity. PEDOT:PSS can be easily processed using various deposition techniques. The deposition protocol and the processing additives have a tremendous influence on the electric conductivities, which can range from 10$^{-2}$ to 10$^3$ S cm$^{-1}$.[7] The most widely used additives are high-boiling co-solvents, surfactants, (i.e. dimethyl sulfoxide, ethylene glycol, or Zonyl®), which lead to more ordered PEDOT domains and higher conductivities.[8] However, in contrast to the conjugated PEDOT, saturated PSS is insulating, hindering charge transport. By stripping the PSS from the deposited PEDOT:PSS film, it is possible to increase the weight fraction of conducting PEDOT in the film, leading to significantly improved conductivities of around 1,000 S cm$^{-1}$.[4] The electronic properties
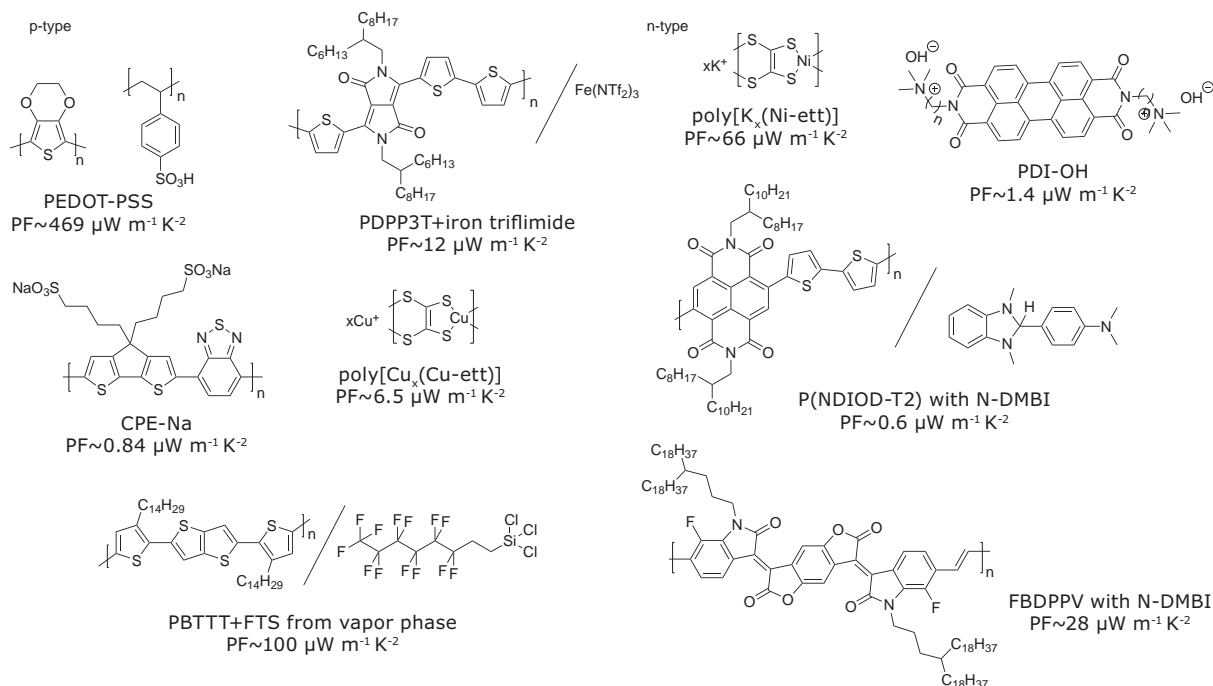


**Figure 2.** Representative p-type and n-type semiconducting polymers and dopants.

of PEDOT:PSS can be further enhanced by carefully controlling the film deposition, thereby gaining control over the phase separation in the PEDOT:PSS film and reducing disorder along the PEDOT backbone, resulting in record conductivities of 4,600 (±100) S cm$^{-1}$.[9] The continually improving conductivities of PEDOT:PSS have also increased its prospect for thermoelectric applications. The ease with which PEDOT films can be doped and dedoped offers an ideal processing handle to tune not only the electrical conductivities, but also the Seebeck coefficients. Crispin et al. reported impressive power factors of 300 µW m$^{-1}$ K$^{-2}$ and ZT values of 0.25, after dedoping highly conductive PEDOT:tosylate with tetrakis(dimethylamino)ethylene (**Cat. No. 674613**).[10] Besides dedoping PEDOT:PSS, the addition of carbon nanotubes or graphene is a popular approach to modulate the thermoelectric properties.[11] By carefully structuring the composite film, conductivities of 10$^5$ S m$^{-1}$ and Seebeck coefficients of 120 µV K$^{-1}$ were measured, leading to thermoelectric power factors of 2710 µW m$^{-1}$ K$^{-2}$, one of the highest values reported for organic thermoelectric materials.[12]

While the p-doping of organic semiconductors can be readily achieved, n-doping is more difficult. Organic electron deficient semiconductors are associated with the high electron affinities (–3 to –4 eV), making the negatively charged molecules prone to reactions with environmental moisture or oxygen.[13,14] Charge transfer salts were among the first organic n-type conductors exploited for thermoelectric applications. The co-crystal of tetrathiafulvalene (TTF) and tetracyanoquinodimethane (TCNQ) is probably the most studied charge transfer salt that exhibited promising thermoelectric properties. Electrical conductivities of 500 S cm$^{-1}$ and power factors of up to 40 µW m$^{-1}$ K$^{-1}$ were obtained. However, several drawbacks significantly limit the applicability of charge transfer crystals as thermoelectric materials. First, modulating the carrier densities is difficult, because the stoichiometry of the co-crystals must be meticulously respected, leaving very little room for composition alterations. Second, the physical properties of the co-crystals are not isotropic, but are highly dependent on the different crystal axes.[15] Alternative approaches to developing n-type conductors for thermoelectric applications have mainly focussed on the perylenediimide and naphtalenediimide containing organic semiconductors. Segalman et al. developed a series of perylene diimide (PDI) based molecular semiconductors functionalized with tertiary amine-containing side chains.[16] Upon thermal annealing, the functionalized PDI moieties self-dope via a dehydration reaction of the tethered tertiary ammonium hydroxide. Interestingly, the self-doped PDI compounds exhibited respectable ambient stability and thermoelectric properties.[17] By carefully designing the side chains, the self-doped PDI moieties achieve conductivities of 0.5 S cm$^{-1}$ and power factors as high as 1.4 µW m$^{-1}$ K$^{-2}$. Based on the complex X-ray diffraction patterns of the self-doped PDIs, the charge carrier transport is most likely limited by inter-crystalline defects, leaving ample room for material optimization. Chabinyc et al. extrinsically doped the high performing n-type polymer poly(*N*,*N*′-bis(2- octyl-dodecyl)-1,4,5,8-napthalenedicarboximide-2,6-diyl]-alt-5,5′-(2,2′-bithiophene)) (P(NDIOD-T2, **Cat. No. 900961**) with the

molecular dopant (4-(1,3-dimethyl-2,3-dihydro-1*H*-benzoimidazol-2-yl)phenyl) (N-DMBI, **Cat. No. 776734**).[18] While the conductivity initially increases as a function of dopant loading, a sharp drop in conductivity is observed at higher loadings. The miscibility of the N-DMBI dopant in the polymer phase is limited, which is why at higher dopant loadings, the dopant crystallizes and phase separates from the polymer matrix, thereby reducing the doping efficiency. Despite the morphological instabilities, Seebeck coefficients of –850 µV K$^{-1}$ have been achieved with power factors of 0.6 µW m$^{-1}$ K$^{-2}$. In a recent report, Pei et al. showed that BDOPV-based FBDPPV polymers have reached a record power factor of 28 µW m$^{-1}$ K$^{-2}$.[19] More interestingly, Huang et al. reported that thiophene-diketopyrrolopyrrole-based quinoidal (TDPPQ) can exhibit a high power factor of 113 µW m$^{-1}$ K$^{-2}$, when the material is interfacially doped by the bismuth. The performance is a record value for reported n-type small molecules.[20]

## Progress in Organic Thermoelectric Devices

Even though the main research efforts in organic thermoelectrics still focus on the development of state-of-the-art materials, device engineering is an important avenue of investigation for organic thermoelectrics for two main reasons. Although power factor and ZT values are widely applied to study the structure-property relationship of organic materials, the output power of devices offers an ultimate way to evaluate thermoelectric performance and clarify related relationships. Moreover, from the point of application-motivated research, the conversion efficiency of a thermoelectric device is strongly dependent on device geometry and the interface property. Therefore, novel designs of device geometry, construction of flexible thermoelectric modules, and development of solution processing (roll-to-roll and ink-jet printing) techniques can boost the power generation, Peltier cooling, and many other applications.

Until now, only a few power generators based on organic materials have been demonstrated. As an example, Crispin et al. reported an organic power generator consisting of 55 legs in a vertical architecture.[21] For this device, a leg with a dimension of 1 × 1.5 × 0.03 mm$^3$ is fabricated by filling cavities with precursor solutions with micropipettes. It should be noted that p-legs are composed of PEDOT-Tos deposited by chemical polymerization of EDOT, while the n-legs are composed of a blend of TTF-TCNQ with PVC. The thermoelectric module exhibits a maximum power output of 0.128 µW at DT of 10 K. Despite this interesting result, further improvement of the power is limited by the low ZT value of the n-type materials and small DT because of limited thickness. Another organic thermoelectric power generator in vertical geometry was reported by Zhu's group.[22] By using metal-organic conducting polymers such as poly-(metal 1,1,2,2-ethenetetrathiolate) as the n-type and p-type materials, large legs with dimensions of 5 × 2 × 0.9 mm$^3$ were fabricated by pressing the polymer powder into pellets. In this way the thermoelectric module serves as a robust device for high power generation. Benefiting from legs with more balanced thermoelectric performance and increased thickness, a thermoelectric module consisting of 35 legs generated a

maximum power and VOC of 750 µW and 0.26 V, respectively, when the DT is maintained at 82 K. The power output density reached 1.2 µW cm$^{-2}$ at 30 K.

Construction of flexible thermoelectric prototype modules is of vital importance for practical applications of organic thermoelectric materials. Recently, Zhu et al. demonstrated a highly integrated flexible module with 220 legs.[23] The prototype device showed an open voltage of 1.51 V and a short current of 2.71 mA. The maximum power output exceeded 1 mW, which is the best performance for organic thermoelectric module published to date. The relative high output voltage and large power output of the constructed module were even sufficient to independently drive a calculator with liquid crystal display. Interestingly, Fujifilm Corporation recently demonstrated a flexible thermoelectric converter[24] with a power generation capacity of few milliwatts capable of generating electricity with a temperature difference of only 1 K. The temperature difference resulting from placing a hand on the device creates enough electricity to power a toy car. It is expected the module will be used as a wearable power supply for a health monitoring device and will incorporate other integrated elements that harvest energy.

In addition to the conventional power generators, organic thermoelectric devices for multifunctional applications have recently attracted increased attention. For instance, organic thermoelectric devices can also be utilized to harvest light energy directly to serve as photo-thermo-electric (PTE) converters. In two recent works done by Kim et al. and Huang et al., PTE devices based on photoselenophene derivatives, (hexyl-3,4-ethyl-enedioxyselenophene, EDOS-C6) and poly[Cux(Cu-ett)], have been constructed independently.[25,26] For these PTE devices, both photothermal (PT) and heat driven thermoelectric

conversion can occur in a single element to allow PTE conversion. As for the EDOS-C6 based device, a high Seebeck voltage of up to 900 µV under moderate NIR light exposure (808 nm @ 2.33 W cm$^{-2}$) can be obtained. In addition to this PTE conversion, photoinduced excitation of the organic active materials can also occur, with an obvious influence on the thermoelectric properties. In Huang's work, the NIR light irradiation on the poly[Cux(Cu-ett)]:PVDF film induced enhancement of the Seebeck coefficient from 52 ± 1.5 to 79 ±5.0 µV K$^{-1}$. Benefitting from prominent PTE and PTE effects of poly[Cux(Cu-ett)]:PVDF, allows for a PTE voltage of 12 mV to be obtained. This enables promising applications of organic TE materials in electricity generation from solar energy and NIR detection.

Sensing is another interesting area of application for organic thermoelectric materials. In that regard, thermoelectric devices represent good candidates for temperature sensors. Interestingly, recent work by Zhang et al. demonstrated the microstructure-frame-supported organic thermoelectric material (MFOTE) can also be applied as pressure-temperature dual-parameter sensors for self-powered e-skin applications.[27] In this device, the temperature difference between the device and object is detected by the Seebeck effect, while the biased pressure can be probed by the change in device resistance. The incorporation of piezoresistive and thermoelectric mechanisms enables the simultaneous detection of temperature and pressure stimuli without an additional decoupling process, and even features a self-powered pressure sensitivity and temperature-sensing accuracy of >20 kPa$^{-1}$ and <0.1 K, respectively. It should be noted the flexible dual-parameter sensor can be self-powered and integrated into array, enabling their intelligent application in a wide range of robotics and health-monitoring products.
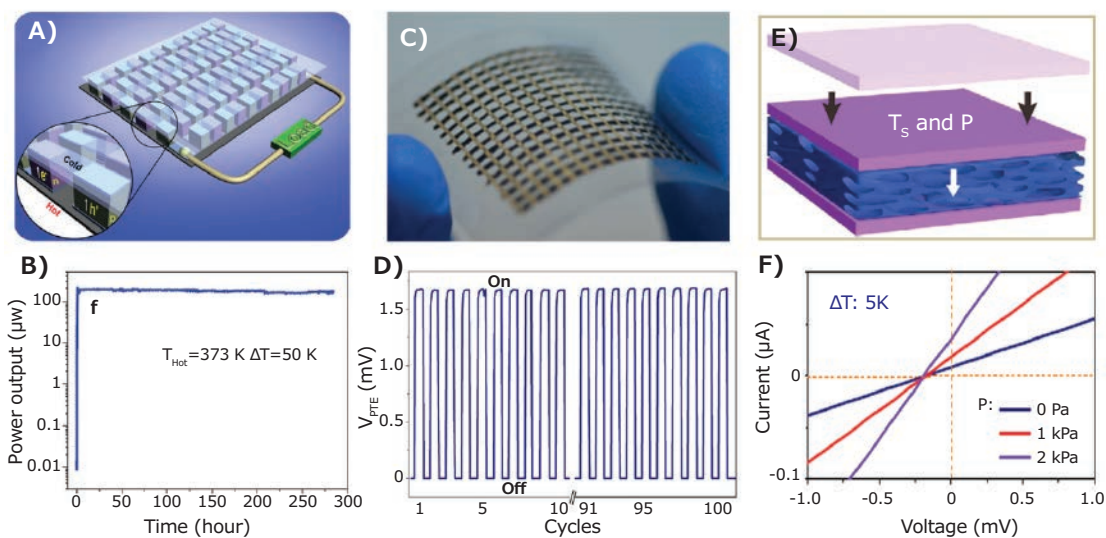


**Figure 3.** A) Schematic illustration of the thermoelectric module. B) Power output stability of the thermoelectric module operating with Thot = 373 K and Δ T = 50 K. C) Photo images of flexible NIR detectors based on PTE effect. D) NIR detection cyclability of flexible device under a laser intensity of 2.3 W.cm$^{-2}$. E) Schematic illustration of temperature–pressure based on MFSOTE devices. F) I–V curves of a MFSOTE device at different loading pressure with the temperature gradient of 5 K. Adapted from ref 22 with permission

## Conclusion and Perspectives

After rapid development in the past few years, the field of organic thermoelectrics has made remarkable advancements. High ZT values of >0.2 at room temperature have been successfully demonstrated using both p-type (PEDOT:PSS) and n-type (Poly[Kx(Ni-ett)]) materials. This performance is comparable to those of many inorganic counterparts at low temperatures. Moreover, several organic thermoelectric devices have been fabricated using printing methods, indicating rapid progress of this cutting-edge field.

Despite these achievements, organic thermoelectrics are still in the initial development stage and face a number of challenges. One challenge is the need to identify more organic thermoelectric materials with high ZT value. Until now, only limited organic candidates have been explored in thermoelectric studies, leaving the investigation of structure-property relationship an open question. An in-depth understanding of the critical roles of a conjugated backbone, side chains, polymer molecular weight, and energy levels will enable development of state-of-the-art organic thermoelectric materials. Many high-mobility organic semiconductors are good candidates for thermoelectric applications by principle. In general, their low carrier density limits the improvement of electrical conductivity, impeding their use in thermoelectrics. Controlling charge carrier concentration in organic semiconductors emerges as a key challenge; therefore development of high efficient doping methods will accelerate the achievement of high performance thermoelectronics from organic semiconductors.

The second challenge is lack of understanding of the fundamental mechanisms of organic thermoelectrics. The combined effect of many physical processes, including charge transport, phonon transport, and phonon scattering are involved in thermoelectric conversion and lead to a complicated operating mechanism. There are a number of important questions to be answered. For example, what kind of charges dominate the charge transport organic materials from the standpoint of charge transport? What is the best model for intrinsic charge transport in various organic semiconductors and their doped systems? How can we better characterize the important role of carriers and phonons in determining the thermal transport property of organic semiconductors? Furthermore, the S-σ trade-off relationship, σ-$k$ relationship, and the relationship between energy level and S constitute several questions for organic thermoelectric materials, which require further investigation. Understanding these mechanisms and reconciliation of the trade-off relationships remain challenging tasks.

The development of flexible organic thermoelectric devices with high power generation density constitutes the third challenge. The output power of organic thermoelectric devices is not only governed by the properties of materials, but also strongly related to the condensed structure of the material and the properties of their interfaces with electrodes. Precisely modulated micro/nano-structure and functional interfaces deserve focused attention to maximize the output power of the device. Another opportunity relies on the construction of flexible devices for low-cost applications. To meet this requirement, flexible integrated modules consisting of a huge number of thermoelectric legs should be fabricated utilizing solution-processing techniques. However, both device geometry and integration of organic thermoelectric devices are not well developed.

Precise measurement of key thermoelectric parameters including S, σ, and $k$ constitutes the fourth challenge in organic thermoelectrics. While characterization techniques are established for inorganic thermoelectrics, a standard protocol for organic thermoelectric materials does not exist. To ensure thermoelectric performance is accurately evaluated, the size and shape of organic materials and electrodes, as well as the properties of the substrate must be clearly reported. It should be noted the power factor is usually utilized to evaluate the performance of organic materials, since in-plane thermal conductivity cannot be obtained in a straightforward way. Although the 3ω method has been adopted for organic thermoelectric materials in the past few years, the difficulties in device fabrication and measurement setup makes wide acceptance of this method difficult.

## References

(1) https://energy.gov/eere/amo/articles/waste-heat-recovery-resource-page
(2) Snyder, G. J.; Toberer, E. S. *Nat. Mater*. **2008**, *7*, 105.
(3) Wang, H.; Hsu, J. H.; Yi, S. I.; Kim, S. L.; Choi, K.; Yang, G.; Yu, C. *Adv. Mater*. **2015**, *27*, 6855.
(4) Kim, G. H.; Shao, L.; Zhang, K.; Pipe, K. P. *Nat. Mater*. **2013**, *12*, 719.
(5) Bubnova, O.; Crispin, X. *Energ. Environ. Sci*. **2012**, *5*, 9345.
(6) Cowen, L. M.; Atoyo, J.; Carnie, M. J.; Baran, D.; Schroeder, B. C. *ECS J. Solid State Sci. Technol.* **2017**, *6*, N3080.
(7) Shi, H.; Liu, C.; Jiang, Q.; Xu, J. *Adv. Electron. Mater*. **2015**, *1*, 1500017.
(8) Rivnay, J.; Inal, S.; Collins, B. A.; Sessolo, M.; Stavrinidou, E.; Strakosas, X.; Tassone, C.; Delongchamp, D. M.; Malliaras, G. G. *Nat. Commun.* **2016**, *7*, 11287.
(9) Worfolk, B. J.; Andrews, S. C.; Park, S.; Reinspach, J.; Liu, N.; Toney, M. F.; Mannsfeld, S. C. B.; Bao, Z. *Proc. Natl. Acad. Sci.* **2015**, *112*, 14138.
(10) Bubnova, O.; Khan, Z. U.; Malti, A.; Braun, S.; Fahlman, M.; Berggren, M.; Crispin, X. *Nat. Mater.* **2011**, *10*, 429.
(11) Song, H.; Liu, C.; Xu, J.; Jiang, Q.; Shi, H. *RSC Adv.* **2013**, *3*, 22065.
(12) Cho, C.; Wallace, K. L.; Tzeng, P.; Hsu, J.-H.; Yu, C.; Grunlan, J. C. *Adv. Energ. Mater.* **2016**, *6*, 1502168.
(13) Anthopoulos, T. D.; Anyfantis, G. C.; Papavassiliou, G. C.; de Leeuw, D. M. *Appl. Phys. Lett.* **2007**, *90*, 122105.
(14) Zhao, Y.; Guo, Y.; Liu, Y. *Adv. Mater.* **2013**, *25*, 5372.
(15) Kwak, J. F.; Chaikin, P. M.; Russel, A. A.; Garito, A. F.; Heeger, A. J. *Solid State Commun.* **1975**, *16*, 729.
(16) Russ, B.; Robb, M. J.; Brunetti, F. G.; Miller, P. L.; Perry, E. E.; Patel, S. N.; Ho, V.; Chang, W. B.; Urban, J. J.; Chabinyc, M. L.; Hawker, C. J.; Segalman, R. A. *Adv. Mater.* **2014**, *26*, 3473.
(17) Russ, B.; Robb, M. J.; Popere, B. C.; Perry, E. E.; Mai, C.-K.; Fronk, S. L.; Patel, S. N.; Mates, T. E.; Bazan, G. C.; Urban, J. J.; Chabinyc, M. L.; Hawker, C. J.; Segalman, R. A. *Chem. Sci.* **2016**, *7*, 1914.
(18) Schlitz, R. A.; Brunetti, F. G.; Glaudell, A. M.; Miller, P. L.; Brady, M. A.; Takacs, C. J.; Hawker, C. J.; Chabinyc, M. L. *Adv. Mater.* **2014**, *26*, 2825.
(19) Shi, K.; Zhang, F.; Di, C. A.; Yan, T. W.; Zou, Y.; Zhou, X.; Zhu, D.; Wang, J. Y.; Pei, J. *J. Am. Chem. Soc.* **2015**, *137*, 6979.
(20) Huang, D.; Wang, C.; Zou, Y.; Shen, X.; Zang, Y.; Shen, H.; Gao, X.; Yi, Y.; Xu, W.; Di, C. A.; Zhu, D. *Angew. Chemie. Int. Ed.* **2016**, *55*, 10672.
(21) Bubnova, O.; Khan, Z. U.; Malti, A.; Braun, S.; Fahlman, M.; Berggren, M.; Crispin, X. *Nat. Mater.* **2011**, *10*, 429.
(22) Sun, Y.; Sheng, P.; Di, C.; Jiao, F.; Xu, W.; Qiu, D.; Zhu, D. *Adv. Mater.* **2012**, *24*, 932.
(23) Sheng, P.; Sun, Y.; Jiao, F.; Di, C.; Xu, W.; Zhu, D. *Synth. Met.* **2014**, *193*, 1.
(24) Hideyoshi, K. http://techon.nikkeibp.co.jp/english/NEWS_EN/20130206/264517/
(25) Huang, D.; Zou, Y.; Jiao, F.; Zhang, F.; Zang, Y.; Di, C. A.; Xu, W.; Zhu, D. *ACS Appl. Mater. Interfaces* **2015**, *7*, 8968.
(26) Kim, B.; Shin, H.; Park, T.; Lim, H.; Kim, E. *Adv. Mater.* **2013**, *25*, 5483.
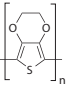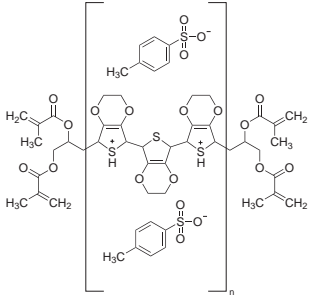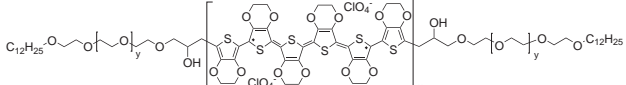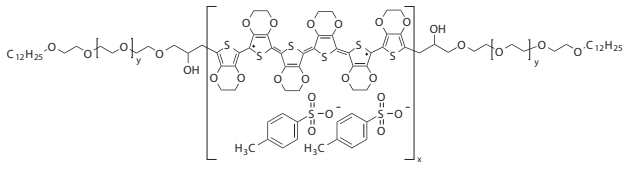(27) Zhang, F.; Zang, Y.; Huang, D.; Di, C.; Zhu, D. *Nat. Commun.* **2015**, *6*, 8356.

## Poly(3,4-ethylenedioxythiophene):poly(styrenesulfonate) (PEDOT:PSS)

For a complete list of available materials, visit **SigmaAldrich.com/pedot**.

| Description | Sheet Resistance (Ω/sq) | Viscosity | pH | Cat. No. |
|---|---|---|---|---|
| dry re-dispersible pellets, high conductivity | <200 (by addition of 5% diethylene glycol) | - | - | **900208-1G** |
| dry re-dispersible pellets | 200-450 | - | - | **768618-1G** <br> **768618-5G** |
| 0.8% in $H_2O$, conductive inkjet ink | - | 7-12 cP at 22 °C | 1.5 - 2.5 | **739316-25G** |
| 5.0 wt. %, conductive screen printable ink | 50-150 | 30,000-90,000 mPa.s at 22 °C | 1.5 - 2.0 | **768650-25G** |
| 1.1% in $H_2O$, neutral pH high-conductivity grade | <100 (>70% visible light transmission, 40 μm wet) | <100 cP at 22 °C | 5 - 7 | **739324-100G** |
| 1.1% in $H_2O$, surfactant-free, high-conductivity grade | <100 (<80% visible light transmission, 40 μm wet) | 30-100 cP at 20 °C | <2.5 | **739332-100G** |
| 1.0 wt. % in $H_2O$, high-conductivity grade | 50-120 | 7-12 mPa.s at 22 °C (typical) | 1.8 - 2.2 | **768642-25G** |
| high-conductivity grade | <200 (coating : 40 μ wet, drying: 6 min 130 °C) | <30 mPa.s at 20 °C | - | **900181-100G** |
| 2.8 wt % dispersion in $H_2O$, low-conductivity grade | - | <20 cP at 20 °C | 1.2 - 1.8 | **560596-25G** <br> **560596-100G** |
| 3.0-4.0% in $H_2O$, high-conductivity grade | 500 (4 point probe measurement of dried coating based on initial 18 μm wet thickness.) <br> 1500 (4 point probe measurement of dried coating based on initial 6 μm wet thickness.) | 10-30 cP at 20 °C | 1.5 - 2.5 at 25 °C (dried coatings) | **655201-5G** <br> **655201-25G** |

## Other PEDOTs

For a complete list of available materials, visit **SigmaAldrich.com/polythio**.

| Name | Structure | Description | Conductivity | Cat. No. |
|---|---|---|---|---|
| Poly(3,4-ethylene-dioxythiophene) |  | in $H_2O$, dodecylbenzene sulfonic acid (DBSA) as dopant | - | **675288-25ML** |
| Poly(3,4-ethylene-dioxythiophene), tetramethacrylate end-capped |  | 0.5 wt. % (dispersion in propylene carbonate), p-toluenesulfonate as dopant | 0.1-0.5 S/cm (bulk) | **649813-25G** |
| | | 0.5 wt. % (dispersion in nitromethane), p-toluenesulfonate as dopant | 0.1-0.5 S/cm (bulk) | **649821-25G** |
| Poly(3,4-ethylenedioxy-thiophene), bis-poly(ethyleneglycol), lauryl terminated |  | 0.8 wt. % (dispersion in propylene carbonate) 0.6-1.1 wt. %, perchlorate as dopant | 10-45 S/cm (bulk) | **736287-25G** |
| Poly(3,4-ethylenedioxy-thiophene), bis-poly(ethyleneglycol), lauryl terminated |  | 0.6-1.0 wt. % (solid) 0.8 wt. % (dispersion in 1,2-dichlorobenzene), p-toluenesulfonate as dopant | 0.01-0.05 S/cm (bulk) | **736309-25G** |
| | | 0.7 wt. % (dispersion in nitromethane) 0.5-0.9 wt. % (solid concentration), p-toluenesulfonate as dopant | $10^{-2}$-$10^{-4}$ S/cm (bulk) | **736295-25G** |

# MilliporeSigma

# TRANSPARENT CONDUCTIVE CNT INKS

**Printable** ⏐ **Environmentally Stable** ⏐ **Stretchable**

Formulated using patented CoMoCAT™ CNTs, aqueous and solvent-based (V2V™) conductive inks are setting a new standard for transparent conductor performance in applications where durability and environmental stability are paramount.
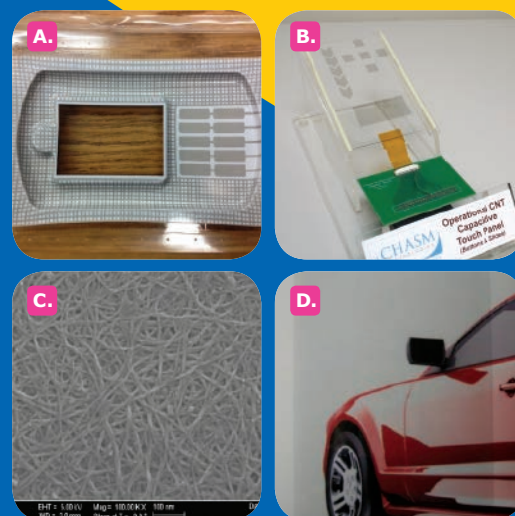
A. Thermoformed CNT touch sensor prototype
B. Capacitive CNT touch screen array
C. CNT TCF at 95% VLT
D. TEM scan of rod-coated CNT network (~10 mg/mm²)

## V2V™: Print. Dry. Done.

**Conductive CNT Ink Systems are optimized for screen printing:**
- Dries quickly, evenly at low temperature
- Contains no surfactants or electrically active dispersants, binders[1]
- Adheres strongly to common screen printing substrates

## Conductive CNT Inks

| | Description | Purpose | Sheet Resistance[2] (Ω/sq) | | | Cat. No. |
|---|---|---|---|---|---|---|
| | | | **85% VLT** | **90% VLT** | **92% VLT** | |
| AC100 | SWCNT in aqueous surfactant solution | Spray Coating | 137 | 237 | 330 | **791490** |
| AC200 | SWCNT in aqueous surfactant solution | Meyer-Rod/Slot-Die Coating | 166 | 251 | 317 | **791504** |
| VC101 | SWCNT in proprietary solvent system (V2V) | Screen Printing | 783 | 1,466 | 2,206 | **792462** |

1. V2V inks (e.g., VC101) contain electrically inert sulfonated tetrafluoroethylene (Nafion).
2. SR measurements for AC100, 200 taken with top coat.

For detailed product information on Conductive CNT inks, visit **SigmaAldrich.com/swnt**.

**Sigma–Aldrich**®
Lab Materials & Supplies

# THE MASTERS OF MATERIALS

**Expertise at the nanoscale**

**www.SigmaAldrich.com/nanomaterials**

**MilliporeSigma**